Contributions to Geophysics and Geodesy Vol. 55/2, 2025 (223–264)

Estimation of the effective elastic thickness using global gravitational, lithospheric structure, and rheology models

Robert TENZER[1,*], Mehdi ESHAGH[2], Samurdhika RATHNAYAKE[2]

[1] Department of Land Surveying and Geo-Informatics, Hong Kong Polytechnic University, 181 Chatham Road South, Kowloon, Hong Kong

[2] New Technologies for the Information Society (NTIS), Faculty of Applied Sciences, University of West Bohemia, Univerzitní 22, Plzen, Czech Republic

Abstract: Geodetic satellite missions become essential tools to predict the ocean-floor relief and study the oceanic lithosphere. Satellite-altimetry measurements of the sea surface topography are converted to marine gravity values that are used to predict bathymetric depths. This procedure requires information on marine sediment deposits as well as the lithospheric elastic thickness. Moreover, the elastic thickness provides information on the lithospheric strength in the context of interpreting tectonism and geological processes. In this study, we estimated the lithospheric elastic thickness beneath the Indian Ocean and surrounding continental regions by applying two methods that determine this parameter individually for the oceanic and continental lithosphere. For the former, we used global lithospheric age and upper-mantle temperature models. For the latter, we derived this parameter using global gravitational, lithospheric structure, and rheology models. Since our estimates are based on global models, the resulting map of the elastic thickness lacks more detailed features of lithospheric strength. Nevertheless, the principal pattern in elastic thickness variations relatively closely resemble tectonic configuration and lithospheric thermal state beneath the Indian Ocean. Active divergent tectonic margins along mid-oceanic rifts are characterized by a weak lithospheric strength. The strength increases due to cooling of the oceanic lithosphere with its age, while reaching maxima ~50 km. A relatively weak lithosphere is found beneath Madagascar (15–30 km) and Sri Lanka (24–35 km). Within the domain of the Indian Ocean, the maximum elastic thickness (~130 km) is detected beneath continental crustal fragments of the South Kerguelen Plateau.

Key words: elastic thickness; flexure, isostasy; lithosphere; active tectonic margins, Indian Ocean

*corresponding author, e-mail: robert.tenzer@polyu.edu.hk; phone: +852 2766-5592

doi: 10.31577/congeo.2025.55.2.6

1. Introduction

The (effective) elastic thickness describes a lithospheric strength that depends on many factors (e.g., *Lowry and Smith, 1995; Burov and Diament, 1995, 1996; Pérez-Gussinyé et al., 2004; Pérez-Gussinyé and Watts, 2005*). According to early loading studies (e.g., *Watts et al., 1980*), the strength of the oceanic lithosphere is mainly controlled by its thermal state due to conductive cooling. In addition, variations in rheological properties (e.g., grain size evolution, hydration and melt state, thermal perturbations to a plate cooling model that must result from advective transport processes and small-scale convection) as well as the state of flexural bending and tectonic stresses partially affect the strength of the oceanic lithosphere. Other factors are associated with magmatism at hotspots in combination with the ocean-floor spreading and a load of volcanic formations. Whereas thermal gradient substantially controls the strength of the oceanic lithosphere, the elastic thickness of the continental lithosphere depends not only on its thermal state, but eventually also on its composition. Estimates of the continental elastic thickness show large variations within plates of the same thermo-tectonic age (cf. *Burov and Diament, 1996*). In principle, old tectonic provinces (>1.5 Ga) are formed by a colder and thicker lithosphere, more depleted in basaltic constituents, thus more dehydrated than younger formations (e.g., *Jordan, 1979*). Studies by *Simons et al. (2003)*, *Flück et al. (2003)*, *Swain and Kirby (2003; 2006)*, *Pérez-Gussinyé and Watts (2005)*, *Pérez-Gussinyé et al. (2007; 2009b)*, *Tassara et al. (2007)*, *Audet and Bürgmann (2011)*, *Tesauro et al. (2013)*, and others suggested a possible existence of a large elastic thickness (>60 km) of older geological provinces with the lithospheric thickness significantly exceeding estimates for younger formations. These findings suggest that continental cratonic interiors are more resilient to deformations (e.g., *Tesauro et al., 2013*). Other factors, on the other hand, act reversely in time. Along active orogenic belts, for instance, the lithosphere becomes weaker in time due to a crustal thickening as well as flexural stresses caused by a lithospheric bending due to topographic and horizontal tectonic loads (e.g., *Eshagh et al., 2020*). Consequently, a thick continental crust becomes sufficiently hot to reduce considerably its strength. This process results in a mechanical decoupling of the crust from the lithospheric mantle, leading to a significant lithospheric weakening (e.g., *Burov and Diament, 1996*). Other factors, such as reheating and hydrating of the lithospheric mantle, occurring in continental mobile mountain belts located in back-arc regions, could decrease the elastic thickness of the continental lithosphere (e.g., *Hyndman et al., 2005*). The extensional tectonism along active continental rift systems typically also weakens a lower crust, leading to a subsequent crust-mantle decoupling and a lithospheric weakening (cf. *Cloetingh and Burov, 1996; Burov, 2011*). Inherently, the elastic thickness is an important parameter that provides valuable information on the state of lithospheric stresses caused by tectonic and other geological processes. This applies particularly along active convergent tectonic margins where the subduction and orogenic processes significantly change loads on the surface and modulate stresses within the lithosphere (e.g., *Watts, 2001; Tassara et al., 2007*). A lithospheric strength along active divergent tectonic margins is, on the other hand, mainly controlled by a thermal gradient and buoyancy in the hot upper mantle.

Different methods have been developed and applied to estimate the elastic thickness. As stated above, the elastic thickness of the oceanic lithosphere is largely governed by its thermal state. Consequently, it could be theoretically described (in the simplest way) as a function of the ocean-floor age and the oceanic lithospheric temperature. Other methods involve gravity and topographic information (e.g., *Eshagh and Tenzer, 2021*). These methods utilize forward and inverse modelling techniques (*Watts, 2001*). In the forward modelling, loading structures are known and the elastic thickness is estimated by applying a trial-and-error technique. This method is suitable to estimate, for instance, the elastic thickness of seamounts or sedimentary basins. The continental elastic thickness is typically estimated indirectly using a cross-spectral analysis (i.e., admittance or coherence) of gravity and topographic data (e.g., *Eshagh et al., 2020*). This is efficient especially if the lithospheric strength is unknown. A number of authors investigated the continental elastic thickness using the coherence and admittance analysis (*Forsyth, 1985; Poudjom Djomani et al., 1995; Doucouré et al., 1996; McKenzie and Fairhead, 1997; Ojeda and Whitman, 2002; McGovern et al., 2002; Swain and Kirby, 2003; 2006; McKenzie, 2003; Pérez-Gussinyé et al., 2004; 2007; 2009b; Audet and Mareschal, 2004; Gómez-Ortiz et al., 2005; Tassara, 2005; Tassara et al., 2007; Galán and Casallas, 2010*). *Kirby (2014)* provides a comprehensive review of inverse spectral methods.

Artemjev and Kaban (1991) and *McKenzie (2010)* identified inconsistencies between elastic thickness estimates based on applying coherence and admittance analyses. Estimates for cratons based on a transfer function (admittance) between the free-air gravity and topographic data are, in some cases, significantly lower than values obtained from the coherence analysis between the Bouguer gravity and topographic data (e.g., *McKenzie, 2003*). This discrepancy was explained by limitations in applying the admittance method for elevated and actively deforming continental areas (cf. *Artemjev and Kaban, 1991; Burov, 2011*). *McKenzie (2010)* demonstrated that results from the coherence and admittance methods differ by as much as an order of magnitude in continental regions with a flat topography. Similarly, large inconsistencies exist in estimates for the oceanic lithosphere. Many regional studies based on a cross-spectral analysis or isostatic models provide likely unrealistic estimates for the oceanic lithosphere due to disregarding its thermal state.

Topographic and gravity information used solely to estimate the elastic thickness is often insufficient. Some authors considered additional parameters to model a lithospheric strength more realistically. *Tesauro et al. (2013)* took into consideration variations of the Young modulus within the lithosphere. *Chen et al. (2015)* incorporated sediment thickness data into their estimation model. *Tesauro et al. (2018)* accounted for the lithospheric temperature, composition, and strain rates. Alternative methods were also developed based on utilizing isostatic hypotheses (e.g., *Turcotte et al., 1981; Calmant et al., 1990; Filmer et al., 1993; Burov and Diament, 1995; Stewart and Watts, 1997; Braitenberg et al., 2002;* and *Jordan and Watts, 2005*). The isostatic method was developed by *Eshagh (2018)*. He combined flexural and gravimetric isostatic models. Moreover, he incorporated information on a lithospheric density structure (including sediments, underlying crystalline crust, and lithospheric mantle) and crustal thickness variations in addition to rheological properties of the lithosphere to estimate the continental elastic thickness.

In this study, we estimated the elastic thickness of the oceanic and continental lithosphere beneath the Indian Ocean, its marginal seas, and adjoining continental regions. Our motivation was to provide the study of the entire area of interest because most of existing studies focused only on particular regions of a high geological, volcanologic or tectonic importance. Whereas existing regional studies provide more detailed information on lithospheric strength variations within particular study areas, our result provides overall characteristics for the whole ocean. Numerous studies were published for different regions of the Indian Ocean and adjacent areas. Their brief summary is given below (in a geographical rather than chronological order). *Rao et al. (2016)* investigated the lithospheric structure and upper mantle characteristics beneath the Bay of Bengal. *Ratheesh Kumar et al. (2013)* estimated the elastic thickness along the Andaman subduction zone, and *Ratheesh Kumar et al. (2010)* conducted a similar study along the Sumatra-Java oceanic subduction. *Tiwari et al. (2003)* and *Subrahmanyam et al. (2008)* investigated the elastic thickness along the Ninety-East Ridge, and *Sreejith and Krishna (2013)* studied isostatic compensation mechanisms along this ridge. *Chaubey et al. (2008)* studied the isostatic response of the Laccadive Ridge. *Ashalatha et al. (1991)*, *Tiwari et al. (2007)*, *Trivedi et al. (2012)*, and *Sreejith et al. (2019)* extended the study for the whole region of the Chagos-Laccadive Ridge System. *Sreejith et al. (2011)* investigated processes associated with a negative gravity anomaly along the Eighty-Five East Ridge. *Bansal et al. (2005)* studied isostatic mechanisms of the sea-floor relief structures offshore India. *Ratheesh Kumar et al. (2015)* and *Chand and Subrahmanyam (2003)* investigated the elastic thickness beneath the western continental margin of India and the eastern continental margin of Madagascar. Regional geophysical studies dealing with the isostasy and lithospheric strength in the western part of the Indian Ocean were conducted also by *Radha Krishna (1996)*, *Bansal et al. (2005)*, *Tiwari et al. (2007)*, *Ratheesh Kumar and Xiao (2018)*, and *Mishra et al. (2018; 2020)*. *Sreejith et al. (2008)* investigated the structure and isostatic compensation state of the Comorin Ridge. *Kunnummal and Anand (2022)* studied the elastic thickness beneath the Greater Maldive Ridge, comprising the Maldive Ridge and the Deep Sea Channel. *Ratheesh Kumar et al. (2020)* and *Prasanna et al. (2014)* carried out elastic thickness studies of Sri Lanka. *Grevemeyer et al. (2001)* estimated the elastic thickness beneath the Kerguelen Plateau. Studies of the lithospheric strength within the Indian subcontinent were conducted, for instance, by *Ratheesh Kumar et al. (2014)* and *Chen et al. (2015)*. *Shi et al. (2017)* conducted a comprehensive study of elastic thickness variations within Southeast Asia. Among investigations of the lithospheric strength in Africa, Arabian Peninsula, and Iran, we could mention two recent studies by *Eshagh et al. (2020)* and *Gedamu et al. (2021)*.

Regional studies in different parts of the Indian Ocean (summarized above) were mostly done by applying admittance, coherence, and isostatic methods. These methods involved only topographic, bathymetric, and gravity information, while disregarding a thermal state of the oceanic lithosphere. As already explained, this could yield unrealistic results. To address this theoretical deficiency, we applied the method based on a thermal state to estimate the elastic thickness of the oceanic lithosphere. For the continental lithosphere we applied a method developed by *Eshagh (2018)*. It combines gravimetric and flexural isostatic theories and takes into consideration rheological properties.

The study is organised into five sections, beginning with a review of theoretical models in Section 2. A tectonic setting of the study area and input data acquisition are described in Section 3. Results are presented in Section 4, and discussed in Section 5. Major numerical findings are summarized in Section 6.

2. Method

Methods applied to compute the lithospheric elastic thickness are explained in this section. Firstly, the expression to compute this parameter for the oceanic lithosphere is given based on lithospheric age and temperature of upper mantle. The Vening Meinesz-Moritz (VMM) and flexural isostatic models are then briefly recapitulated and a numerical technique of estimating the elastic thickness of the continental lithosphere, including continental margins accommodating sediments, based on combining these two isostatic models is described.

2.1. Elastic thickness of the oceanic lithosphere

Studies of the oceanic lithospheric flexure revealed that the elastic thickness is proportional to the square root of age of the oceanic lithosphere at the time of loading and agrees with the isotherm in the range between 450 and 600 °C (cf. *Watts, 1978; Calmant et al., 1990; Wessel, 1992*). For the considered range of isotherm values and the agreement between the observed and predicted bathymetric depths according to a half-space cooling model (e.g., *Carslaw and Jaeger, 1959*), the elastic thickness T_e of the oceanic lithosphere (in km) has been computed according to the following expression:

$$T_e = 2\sqrt{kt}\,\mathrm{erf}^{-1}\left(\frac{T_{\mathrm{iso}}}{T_m}\right), \tag{1}$$

where T_{iso} is the thermal isotherm, T_m is the upper mantle temperature, k is the parameter of thermal diffusivity, t is the oceanic lithosphereric age (in Ma), and erf^{-1} denotes the inverse of the error function. In our numerical realization, we adopted the following values $T_m = 1250\,^{\circ}\mathrm{C}$, $T_{\mathrm{iso}} = 600\,^{\circ}\mathrm{C}$, and $k = 31.5 \times 10^6$. Global models of upper mantle temperature and lithospheric age were used to obtain the parameters T_m and t.

2.2. Elastic thickness of the continental lithosphere

We combined gravimetric and flexural isostatic theories to estimate the elastic thickness of the continental lithosphere according to the numerical approach proposed by *Eshagh (2018)*. Theoretical definitions of both isostatic theories and their combined solution for deriving the elastic thickness are summarized next.

2.2.1. Gravimetric isostatic principle

According to the VMM isostatic approach, *Eshagh (2016a)* defined a Moho flexure w as follows:

$$\begin{aligned} w = -\frac{1}{4\pi G \Delta\rho} \sum_{n=0}^{\infty} \left(\tfrac{2n+1}{n+1}\right) \beta_n \,\times \\ \times \sum_{m=-n}^{n} \left(\delta g_{nm} - g_{nm}^{T} - g_{nm}^{B} - g_{nm}^{S} - g_{nm}^{C}\right) Y_{nm}(\theta,\lambda)\,, \end{aligned} \tag{2}$$

where G denotes the Newton's (universal) gravitational constant; $\Delta\rho$ is the Moho density contrast; δg_{nm} are the spherical harmonic coefficients of gravity disturbances; g_{nm}^{T}, g_{nm}^{B}, g_{nm}^{S}, and g_{nm}^{C} are, respectively, the spherical harmonic coefficients of topography, bathymetry, sediments, and consolidated crust; and $Y_{nm}(\theta,\lambda)$ are the (surface) spherical harmonics of degree n and order m for arguments of spherical co-latitude θ and longitude λ. The gravitational contribution of the Earth's atmosphere is everywhere less than 1 mGal (cf. *Tenzer and Vajda, 2009*). We note that in polar areas, the ice gravity correction (having maxima of ~300 mGal; cf. *Vajda et al., 2008; Tenzer et al., 2015*) has to be applied in Eq. (2).

A maximum degree of summation in Eq. (2) is typically limited up to degree 180. This spectral resolution roughly corresponds to a spatial resolution of ~110 km (at the equator). *Turcotte and Schubert (2014, p. 252)* mentioned that this spatial resolution represents a limit below which loads are not compensated. In other words, the isostatic mechanism applies at scales roughly exceeding 100 km (e.g., *Eshagh and Tenzer, 2021*). The application of the sediment gravity correction, described by spherical harmonics of sediments on the right-hand side of Eq. (2) accounts for the load of sediments covering large parts of marginal seas, particularly in the Bay of Bengal. The application of this correction for the oceanic lithosphere, defined in Eq. (1), is disregarded. The reason is that the sediment cover of the oceanic lithosphere is typically small. The sediment loading on the oceanic lithosphere is then much less prevalent.

To account for a generally different average thickness of the continental crust, the degree-dependent Moho parameter β_n was applied in Eq. (2). It reads (*Eshagh, 2017*):

$$\beta_n = \left(1 - (n+2)\,\frac{\bar{M}}{2R}\right)^{-1}, \tag{3}$$

where R is the Earth's mean radius, and $\bar{M}$ is the mean Moho depth (typically taken from seismic data).

2.2.2. Flexural isostatic principle

The determination of a compensation depth based on utilizing the flexural isostatic theory requires knowledge of mechanical properties of the lithosphere. Flexural models are formulated based on a loading theory (e.g., *Eshagh et al., 2020*). The lithosphere in these models is exemplified by either an elastic or a viscoelastic spherical shell. *Eshagh (2016a; 2016b)* adopted this theory to derive expressions for a gravimetric modelling of the Moho flexure. This is done by solving the partial differential equation of flexure for a viscoelastic spherical shell. It reads (cf. *Watts 2001, p. 225*):

$$\frac{D}{R^4 g}\nabla^4 w + \Delta\rho\, w = \bar{\rho} H\,, \tag{4}$$

where ∇^2 denotes the Laplacian operator, g is the gravity, $\bar{\rho}H$ is the product of the density and height of a load, and the parameter w denotes a Moho flexure (see also notation used in Eq. (2)). The rigidity of the crust D in Eq. (4) is defined by:

$$D = \frac{ET_e^3}{12\left(1-\nu^2\right)}, \tag{5}$$

where E is the Young modulus, ν is the Poisson ratio, and T_e is the elastic thickness of the continental lithosphere.

In Eq. (4), the partial differential equation of flexure is defined for a spherical shell. *Watts (2001, p. 225)* presented a similar equation, but assuming only a plate shell. To solve the partial differential equation in Eq. (4), the spherical harmonic series is considered for w and $\bar{\rho}H$. We then write:

$$w = \sum_{n=0}^{\infty} \sum_{m=-n}^{n} w_{nm} Y_{nm}\left(\theta,\lambda\right), \tag{6}$$

$$\bar{\rho}H = \sum_{n=0}^{\infty} \sum_{m=-n}^{n} \left(\bar{\rho}H\right)_{nm} Y_{nm}\left(\theta,\lambda\right), \tag{7}$$

where w_{nm} and $\left(\bar{\rho}H\right)_{nm}$ are the spherical harmonic coefficients of w and $\bar{\rho}H$, respectively.

According to *Turcotte et al. (1981)*, we have:

$$\nabla^2 Y_{nm}\left(\theta,\lambda\right) = -n(n+1)\, Y_{nm}\left(\theta,\lambda\right) = -\kappa_n Y_{nm}\left(\theta,\lambda\right). \tag{8}$$

Substituting from Eqs. (6) and (7) back to Eq. (4), the results can be written in terms of spherical harmonics in the following form:

$$\begin{aligned} &\sum_{n=0}^{\infty} \sum_{m=-n}^{n} \left(\bar{\rho}H\right)_{nm} Y_{nm}\left(\theta,\lambda\right) = \\ &\quad = \frac{D}{R^4 g} \nabla^4 \sum_{n=0}^{\infty} \sum_{m=-n}^{n} w_{nm} Y_{nm}\left(\theta,\lambda\right) + \Delta\rho \sum_{n=0}^{\infty} \sum_{m=-n}^{n} w_{nm} Y_{nm}\left(\theta,\lambda\right). \end{aligned} \tag{9}$$

From Eqs. (8) and (9), the solution to the partial differential equation in Eq. (4) is found to be:

$$C_n w_{nm} = \frac{\left(\bar{\rho}H\right)_{nm}}{\Delta\rho}, \tag{10}$$

where

$$C_n = 1 + \frac{D\kappa_n^2}{R^4\, g\, \Delta\rho}\,, \tag{11}$$

$$\kappa_n^2 = n^2(n+1)^2\,. \tag{12}$$

A generic solution of the ordinary differential equation in Eq. (10) is given by (cf. *Eshagh, 2018*):

$$w_{nm} = \frac{(\bar{\rho}H)_{nm}}{C_n\, \Delta\rho}\,. \tag{13}$$

2.2.3. Combined model

The Moho flexure determined from gravimetric and flexural isostasy models should theoretically be the same. Nevertheless, large differences could be found between both results that are caused by a lack of precise information on mechanical properties, mass distribution, and heterogeneity of the lithosphere. So far, some information about these factors has been provided in the CRUST1.0 model (*Laske et al., 2013*). The elastic thickness is a parameter which is not given in this model, but since the Young modulus and the Poisson ratio as well as the geometrical distribution and mass heterogeneity of the crust are given in the model, these parameters could be used to estimate the lithospheric strength. This idea has been incorporated to isostatic theories and used in lithospheric studies (e.g., *Turcotte et al., 1981; Calmant et al., 1990; Filmer et al., 1993; Burov and Diament, 1995; 1996; Stewart and Watts, 1997; Braitenberg et al., 2002; Jordan and Watts, 2005*). In our study, all required parameters for gravimetric and flexural isostasy are taken from the CRUST1.0 model (see also *Eshagh et al., 2020; Eshagh and Pitoňák, 2019*).

The estimation of the elastic thickness of the continental lithosphere by means of combining gravimetric and flexural isostatic models assumes that the results from both models are equal. *Eshagh (2018)* formulated the solution for finding the effective elastic thickness in the following form:

$$\begin{aligned}\sum_{n=0}^{\infty} C_n \sum_{m=-n}^{n} (\bar{\rho}H)_{nm}\, Y_{nm}(\theta,\lambda) &= -\frac{1}{4\pi G} \sum_{n=0}^{\infty} \left(\tfrac{2n+1}{n+1}\right) \beta_n \times \\ &\times \sum_{m=-n}^{n} \left(\delta g_{nm}\delta_{n>N} - g_{nm}^T - g_{nm}^B - g_{nm}^S - g_{nm}^C\right) Y_{nm}(\theta,\lambda)\,,\end{aligned} \tag{14}$$

where the factor $\delta_{n>N}$ is applied to remove long-wavelength harmonics (of a chosen degree N) from a gravity spectrum, so that:

$$\delta_{n>N} = \begin{cases} 1 & n > N \\ 0 & n < N \end{cases} . \tag{15}$$

The purpose of removing a low frequency portion of the gravitational signal is to reduce the signature of deep mantle thermal and structural heterogeneities. *Stewart and Watts (1997)* recommended using $N = 15$ to reduce the effect of sub-lithospheric mantle.

The solution of Eq. (14) is carried out in a forward manner so that different values of the elastic thickness are inserted to Eq. (14) to compute sets of different values of a Moho flexure. The elastic thickness for which the flexure closely agrees with a gravimetric Moho flexure is then selected as a final result (cf. *Eshagh, 2018; Eshagh et al., 2019;* and *Eshagh and Pitoňák, 2019*). Mathematically, this procedure is described as follows:

$$\min_{T_e} \left\| \sum_{n=0}^{\infty} C_n \left(\bar{\rho} H\right)_n + \frac{1}{4\pi G} \sum_{n=0}^{\infty} \left(\tfrac{2n+1}{n+1}\right) \beta_n \times \right. \\ \left. \times \left(\delta g_{nm} \delta_{n>15} - g_{nm}^T - g_{nm}^B - g_{nm}^S - g_{nm}^C\right) \right\| . \tag{16}$$

Mechanical properties of the lithosphere, including the elastic thickness, are incorporated in the compensation coefficient C_n in the first term of this optimization problem. For finding the solution by minimizing Eq. (16), a set of elastic thickness values ranging from 0 to 100 km (or more) is selected with a step-size of 1 km. Then value of the computed norm based on each elastic thickness is plotted. The elastic thickness related to a minimum norm is then selected as the solution; see *Eshagh and Pitoňák (2019)*.

3. Study area and data acquisition

Geological and tectonic setting of the Indian Ocean and input datasets used to estimate the lithospheric elastic thickness are briefly summarized below.

3.1. Geology and tectonic setting of the Indian Ocean

The formation of the Indian Ocean (e.g., *Royer and Sandwell, 1989*) began with the breakup of the Gondwana supercontinent (∼180 Ma ago), the northeast motion of the Indian segment of the Indo-Australian plate (∼125 Ma ago), and its collision with the Eurasian plate (∼50 Ma ago). The separation of the Indo-Australian plate from the Antarctic plate (∼53 Ma ago) constituted the current configuration of the Indian Ocean that occurred since ∼36 Ma ago (e.g., *Forsyth et al., 1987*).

The oceanic lithosphere of the Indian Ocean is divided by major active divergent tectonic margins (see Fig. 1) of the Central, Southwest, and Southeast Indian Ridges (e.g., *Munschy and Schlich, 1989*). The Central Indian Ridge transitions into the Carlsberg Ridge and further extends to the Red Sea-Gulf of Aden Rift System. The Diamantina Fracture Zone is an escarpment formed by the separation of two oceanic plateaus (e.g., *Rathnayake et al., 2019*). The Ninety-East, Eighty-Five East, Madagascar, and Mozambique Ridges form major meridional aseismic ridges including the Chagos-Laccadive Plateau. The ongoing oceanic subduction occurs along the Java-Sunda and Andaman Trenches. The subduction of the Arabian oceanic lithosphere underneath the Eurasian continental lithosphere along the Makran Subduction Zone resulted in the creation of the Makran Accretionary Complex (*Jackson et al., 1995; Vernant et al., 2004*). Major abyssal plains in the Indian Ocean are parts of the Arabian, Somali, Mascarene, Madagascar, Mozambique, Agulhas, and Crozet Basins in the west and the Central Indian, Wharton, Perth, and South Australia Basins (e.g., *Rathnayake et al., 2019*). Hotspots in the Indian Ocean combined with the ocean-floor spreading formed a number of volcanic islands, seamounts, and large igneous provinces. According to pleasurable hypotheses, volcanism at the Réunion hotspot, together with the northward motion of the Indian portion of the Indo-Australian plate, formed the Deccan Traps (e.g., *Torsvik et al., 2013*), the Chagos-Laccadive Plateau (60–45 Ma) (e.g., *Ashalatha et al., 1991*), and the southern part of the Mascarene Plateau (∼45–10 Ma ago). The Kerguelen hotspot formed the Kerguelen Islands and the Kerguelen Plateau, the Ninety-East and Broken Ridges, and the Rajmahal Traps (e.g., *Coffin et al., 2002*). According to *Müller et al. (1993)*, the Marion hotspot is possibly the common cause of volcanism at the Prince Edward islands and the Eighty-Five East Ridge. The Comoro Islands are the results of a tectonic rifting and volcanism at the Comoros hotspot (cf. *Melluso and Morra, 2000; French and Romanowicz, 2015*). For a more detailed tectonic and geological classification of the Indian Ocean we refer readers to the study by *Rathnayake et al. (2019)*.

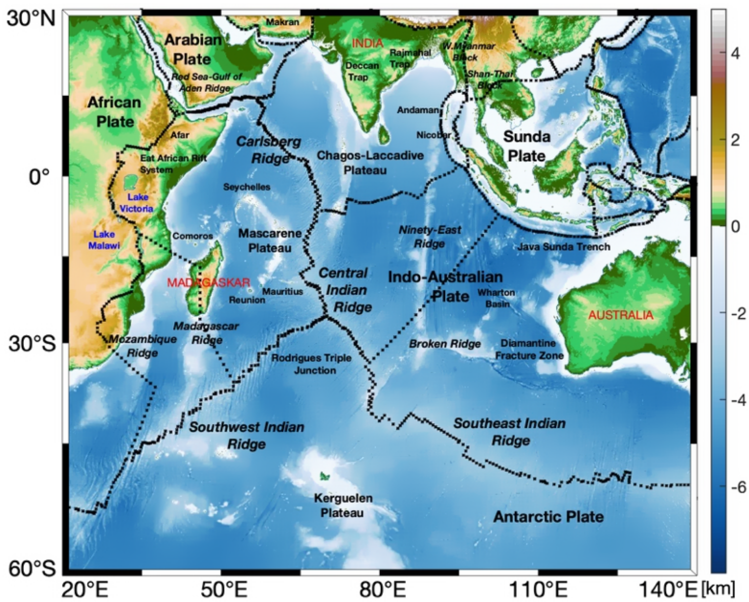

Fig. 1. Solid topography and tectonic setting of the Indian Ocean. Black dotted lines indicate tectonic margins.

3.2. Input data acquisition

We used the TIM_R6e global gravitational model (*Zingerle et al., 2019*) to compile the free-air gravity disturbances with a spectral resolution up to the spherical harmonic degree of 180 (corresponding to a $1^\circ \times 1^\circ$ spatial resolution in terms of a half-wavelength). This model was compiled by augmenting terrestrial gravity observations over polar areas (*Forsberg et al., 2017*) with the satellite-only global gravity field model TIM_R6 (*Brockmann et al., 2019*). The same resolution was used to compute gravity corrections. The gravity disturbance $\delta\boldsymbol{g}$ is defined as the difference between the actual gravity $\boldsymbol{g}$ and the normal gravity $\boldsymbol{\gamma}$, both given at the same point. The gravity anomaly Δg is typically defined as the difference between actual gravity g at the geoid and the normal gravity $\boldsymbol{\gamma}$ at the reference ellipsoid (e.g., *Heiskanen and Moritz, 1967*), while a rigorous definition was given by *Vaníček et al. (2005)*.

The topographic gravity correction was computed using the Earth2014 (*Hirt and Rexer, 2015*) topographic data for the mean topographic density of 2670 kg·m^{-3}. The Earth2014 bathymetric data were used to compute the bathymetric gravity correction for the depth-dependent seawater density model developed by *Gladkikh and Tenzer (2012)*; see also *Tenzer et al. (2011; 2012b)*. The GlobSed (*Straume et al., 2019*) global marine sediment thickness model was used to compute the marine-sediments gravity correction while adopting the marine-sediments density model developed by *Tenzer and Gladkikh (2014)*; see also *Gu et al. (2014)* and *Chen et al. (2014)*. The inland-sediments gravity correction was computed from the CRUST1.0 (*Laske et al., 2013*) sediment thickness and density data. The same model was used to compute the consolidated-crust gravity correction. The gravimetric forward modelling was realised by using expressions derived by *Tenzer et al. (2009a; 2009b; 2011; 2012a; 2015)*, *Tenzer and Chen (2019)*, and modified by *Chen and Tenzer (2020)* to increase their numerical efficiency. The free-air and Bouguer gravity disturbances as well as intermediate results obtained after applying individual gravity corrections to gravity disturbances are plotted in Fig. 2, with the statistical summary in Table 1.

Table 1. Statistics of the (step-wise) corrected gravity disturbances. For notation used, see the legend in Fig. 2.

Gravity correction	**Min** [mGal]	**Max** [mGal]	**Mean** [mGal]	**STD** [mGal]
δg^{FA}	−221	193	−3	34
δg^{T}	−631	191	−23	58
δg^{TB}	−631	756	341	281
δg^{TBS}	−595	772	376	262
δg^{B}	−1029	757	317	328

We used the CRUST1.0 datasets to compute the variable Moho density contrast as the difference between the lateral density variations of the uppermost mantle and the 2900 kg·m^{-3} reference crustal density. We then used the CRUST1.0 Moho depths (defined with respect to the mean sea level) to validate our Moho flexure estimates computed from gravimetric and flexural isostatic models. The Moho depth and density contrast are shown in Fig. 3.

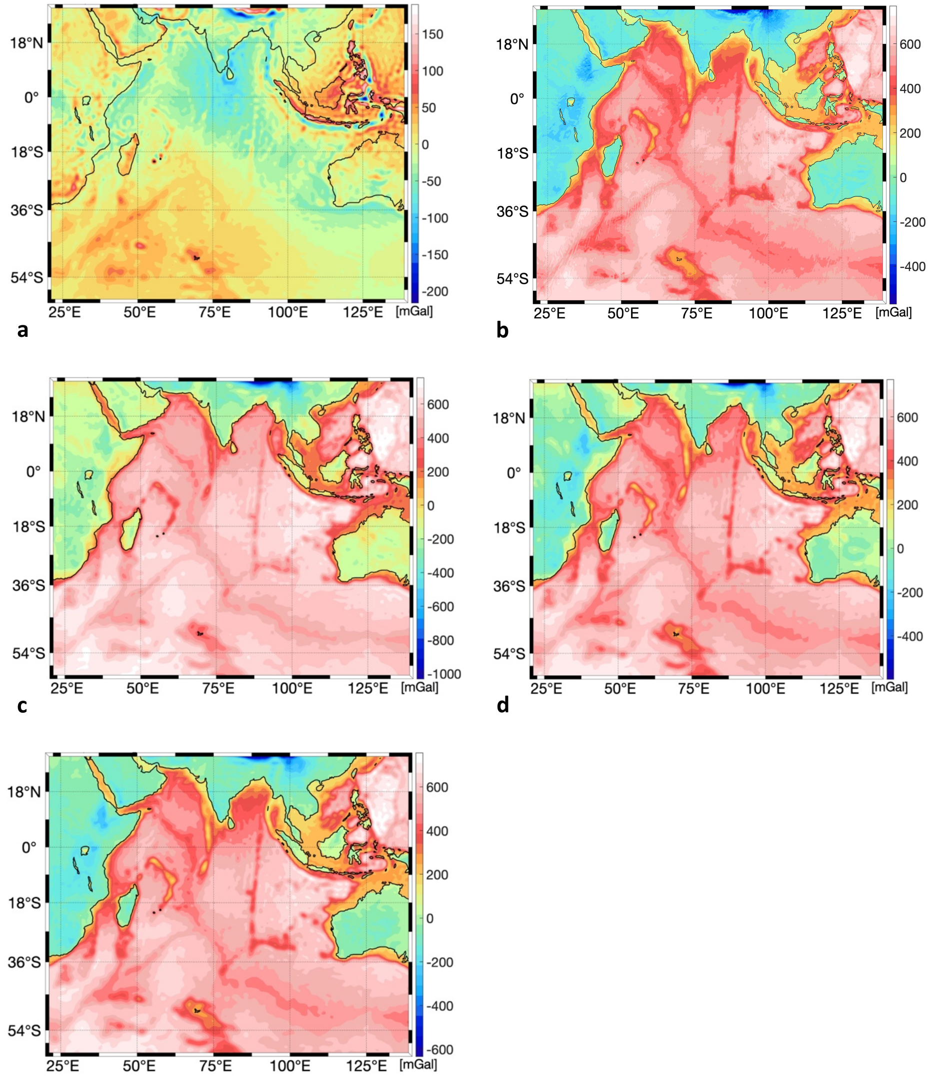

Fig. 2. Gravity maps of the Indian Ocean: (a) the free-air gravity disturbances δg^{FA}, (b) the topography-corrected gravity disturbances δg^{T}, (c) the topography- and bathymetry-corrected gravity disturbances δg^{TB}, (d) the topography-, bathymetry- and sediment-corrected gravity disturbances δg^{TBS} , and (e) the Bouguer gravity disturbances δg^{B}.

The contrast between a thin oceanic crust and a thick continental crust is the most prominent spatial feature in the Moho geometry (Fig. 3a). The minimum Moho depth is detected along mid-oceanic ridges. It moderately increases with the ocean-floor age (or equivalently with age of the oceanic lithosphere). A Moho deepening under volcanic islands, seamounts, and igneous provinces is explained by a regional isostatic signature of these volcanic formations. The Moho density contrast has minima along mid-oceanic ridges (Fig. 3b). This reflects a thermal signature of mantle upwelling. The Moho density contrast again increases with the ocean-floor age (e.g., *Rathnayake et al., 2021*). The Moho density contrast is typically larger under the continental crust, but small values of the Moho density contrast prevail within the Sunda plate that is formed by an assemblage of the continental lithosphere and fragments of the oceanic lithosphere.

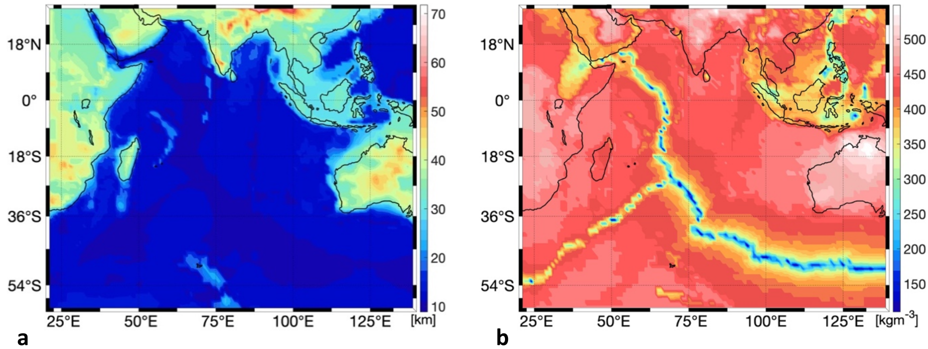

Fig. 3. Maps of: (a) the Moho depth, and (b) the Moho density contrast, both computed from the CRUST1.0 global seismic crustal model.

We used the CRUST1.0 P and S body-wave velocity data to compute the Poisson ratio and the Young modulus (using codes provided by Dr. Michael Bevis that are available at the CRUST1.0 homepage; `https://igppweb.ucsd.edu/~gabi/crust1.html`). Both parameters are shown in Fig. 4 together with the P and S body-wave velocities. Spatial patterns of the Poisson ratio (Fig. 4a) and the Young modulus (Fig. 4b) very closely resemble patterns in seismic velocities (Figs. 4c, d). Minima of both parameters along mid-oceanic ridges correspond with minima of seismic velocities. These minima extend along the northern segment of the East African Rift System, particularly beneath the Afar hotspot. Small values detected within

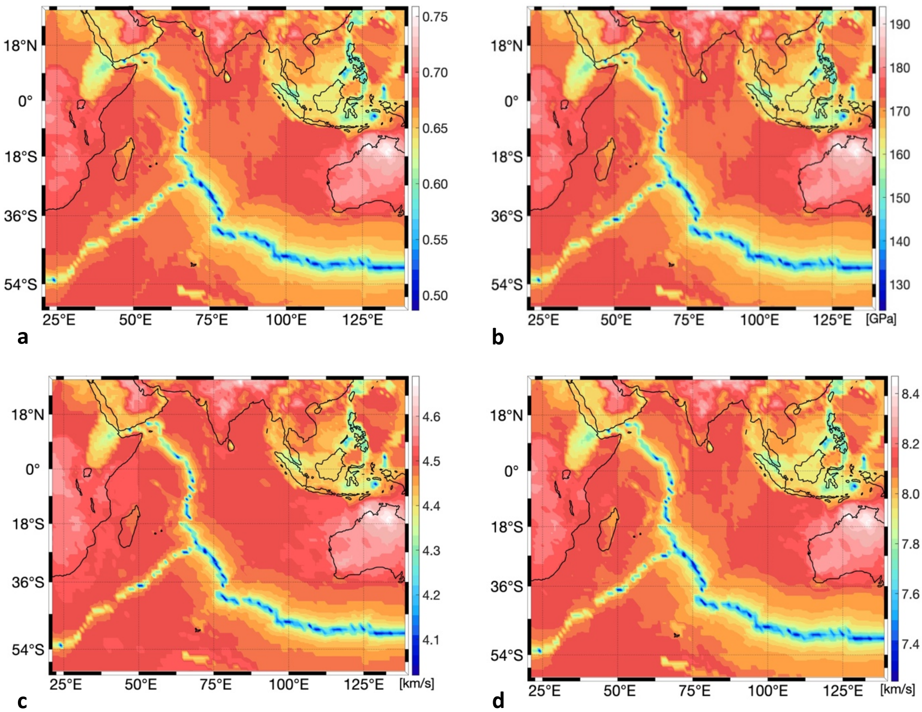

Fig. 4. Maps of: (a) the Poisson ratio, (b) the Young modulus, (c) S-wave velocities, and (d) P-wave velocities.

the Sunda plate reflects volcanism associated with oceanic subductions. As seen Fig. 4, seismic velocities and rheological parameters are mainly controlled by a thermal state of the oceanic lithosphere. This is evident from a prevailing trend of their increasing values with the ocean-floor age. The continental lithosphere is characterized by typically larger values of rheological parameters and seismic velocities. The lithospheric structure of the Arabian Shield (i.e., the western part of the Arabian Peninsula) has much smaller values of the Poisson ratio as well as the Young modulus than the Arabian Platform (i.e., the eastern part of the Arabian Peninsula). This reflects their different thermal state.

The ocean-floor age of the Indian Ocean is shown in Fig. 5a. This updated oceanic crustal age grid together with sets of complementary grids including the spreading rate, asymmetry, direction, and obliquity was pre-

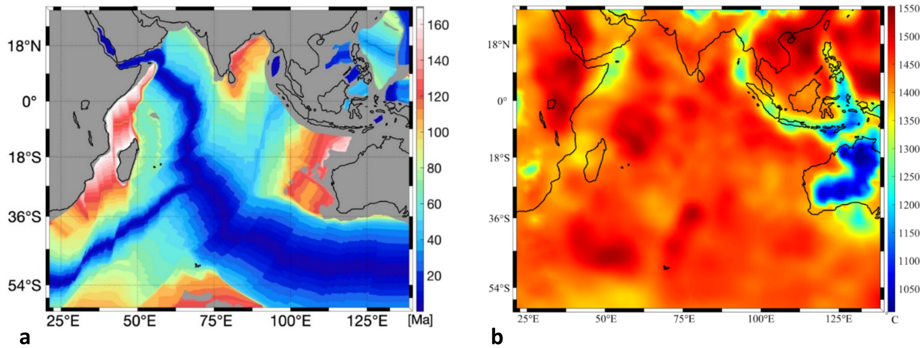

Fig. 5. Maps of: (a) the ocean-floor age, and (b) the upper mantle temperature according to *Seton et al. (2020)*.

pared by *Seton et al. (2020)* based on a selected set of magnetic anomaly identifications and the plate tectonic model of *Müller et al. (2019)*. The upper mantle temperature presented again by *Seton et al. (2020)* is shown in Fig. 5b.

As seen in Fig. 5a, the youngest oceanic lithosphere is along the mid-oceanic ridges, while increasing on both sides of the ridge due to ocean-floor spreading with maximum rates along the Southeast Indian Ridge. Along the Southwest Indian Ridge, the ocean-floor spreading rates are considerably lower. The oldest oceanic lithosphere (>140 Ma) is detected along the east coast of Africa and beneath the Bay of Bengal, the Kerguelen Plateau, and the Diamantina Fracture Zone.

The upper mantle temperature (see Fig. 5b) beneath the Indian Ocean is relatively consistent. Maxima mark locations of the Réunion, Kerguelen, and Marion hotspots. Minima are detected along the Andaman subduction zone. The largest temperature anomalies in West Australia are associated with a low upper mantle temperature beneath the Yilgarn and Pilabara Cratons. The high upper mantle temperature along the Red Sea-Gulf of Aden and East-African Rift Systems is due to a mantle upwelling. A high upper mantle temperature anomaly is also detected beneath the South China Sea.

4. Results

We used data of the ocean-floor age (see Fig. 5a) and the upper mantle temperature (see Fig. 5b) to calculate the elastic thickness of the oceanic lithosphere (Eq. 1), and applied the combined gravimetric-flexural isostatic model (Eq. 14) to estimate it for the continental lithosphere. The elastic thickness of the lithosphere computed on a $1^\circ \times 1^\circ$ sgeographical grid is shown in Fig. 6.

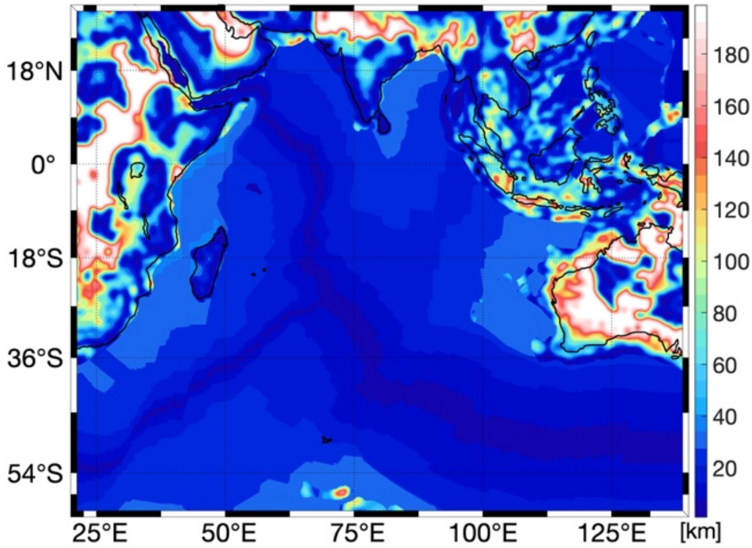

Fig. 6. The effective elastic thickness of the lithosphere beneath the Indian Ocean and surrounding continental areas.

Main features in the spatial pattern of elastic thickness in Fig. 4 are dominated by a significant contrast between typically much larger elastic thickness of the continental lithosphere (with a thick and rigid crust) compared to a low elastic thickness of younger oceanic lithosphere. A newly formed, warm, and less rigid oceanic lithosphere along active mid-oceanic ridges is characterized by a low strength due to flexure and high temperature of the upwelling mantle. The strength of the oceanic lithosphere increases with age due to convective cooling and isostatic rebalance. Large marine sediment deposits along marginal seas, especially at the Bay of Bengal, could modify lithospheric strength but such effect is not apparent in our result. This might be explained by the fact that a partial weakening of the lithosphere attributed to sediment load is somehow compensated by an increasing strength of deep sediment layers due to compaction and further lithification. Much larger elastic thickness variations are detected within the continental lithosphere, with a weaker lithospheric strength along active divergent and convergent continental tectonic margins compared to significant strength of old, cold cratonic formations. A more detailed interpretation of results together with comparison with published studies is given in the next section.

5. Discussion

The result presented in Chapter 4 is discussed and compared with existing studies in the following subsections. We also inspected a possible link between the lithospheric strength, the anomalous gravity pattern, and the crustal geometry (i.e., topography, bathymetry, and crustal thickness).

5.1. Indian Ocean

The lithospheric elastic thickness within the study area varies significantly, with minima $\sim$5 km and maxima exceeding 180 km (Fig. 6). Minima of the elastic thickness ($T_e < 20$ km) are detected along the Central, Southwest, and Southeast Indian Ridges. The minima extend further along the Carlsberg Ridge and the Red Sea-Gulf of Aden Rift System. The elastic thickness gradually increases with an increasing age of the oceanic lithosphere while modifications by the upper mantle temperature (Eq. 1) are not significant. Maxima of the elastic thickness for the oldest parts of the oceanic lithosphere (beneath the Indian Ocean) reach $\sim$50 km offshore West Africa (including the Mozambique Ridge), the Diamantina Fracture Zone (including the Wharton Basin), the Bay of Bengal, and around the Kerguelen Plateau. Within the Indian Ocean, the largest values of the elastic thickness up to $\sim$130 km are detected beneath old, stable continental crustal fragments of the South Kerguelen Plateau.

The Andaman Trench is characterized by a low strength of the lithosphere ($T_e \sim$ 20–25 km) on the side of a subducted slab. The strength further decreases ($T_e \sim$ 8–21 km) beneath the Andaman Sea. The Andaman-Nicobar Archipelago is a sediment-dominated accretionary wedge (i.e., outer-arc islands) associated with a convergent margin tectonic setting (cf. *Bandopadhyay and Carter, 2017*). *Ratheesh Kumar et al. (2013)* investigated the elastic thickness of the Andaman subduction zone using the Bouguer gravity and topographic data and applying the coherence method, specifically by employing the Morlet isostatic response function. They reported the elastic thickness up to ~ 15 km, and minima ($T_e < 3$ km) in the region where the Ninety-East Ridge is close to the Andaman Trench. They also detected a weak lithospheric strength along the ridge. This finding is consistent with the expected signature of an oceanic ridge of a hotspot origin (*Nair et al., 2011*). According to our result, based on taking into consideration a thermal state of this volcanic formation, the elastic thickness there is ~16–32 km. *Tiwari et al. (2003)* reported a more complex pattern in the lithospheric strength along this ridge based on applying the admittance analysis of the free-air gravity and topographic data. According to their results, the elastic thickness along this ridge varies from 22 km in the south to ~17 km in the north, while its central segment has a zero strength ($T_e \sim 0$ km). They proposed that regions with a high lithospheric strength were emplaced on a relatively old lithosphere by an off-ridge intraplate volcanism, and suggested that the southern portion was emplaced over the Antarctic and Australian plates along a fracture zone (see also *Ratheesh Kumar et al., 2013*). They also speculated that a low strength of the central blocks could be due to the interaction of a hotspot with the extinct Wharton spreading ridge. We detected only a much localized circular anomaly of a weak strength in the central part of the ridge that could be explained by a relatively low resolution of our result. *Subrahmanyam et al. (2008)* used a process-oriented approach involving a back stripping of sediments constrained by two seismic profiles across the Ninety-East Ridge. According to their results, the elastic thickness there varies from 1 to 25 km. They interpreted these findings as the evidence for emplacement of the Ninety-East Ridge onto a young oceanic lithosphere close to a mid-oceanic ridge aligned along a fracture zone. *Ratheesh Kumar and Windley (2013)* applied two independent methods, specifically the coherence analysis (based on using the fan-wavelet transform technique) and the flexure inversion with the convolution method, while obtaining results that broadly agree to each other. According to their results, values of the elastic thickness along the ridge are much lower than those characteristic for a normal oceanic lithosphere, thus providing strong support for a hotspot theory. This finding broadly agrees with our result based on age and temperature of the oceanic lithosphere. The elastic thickness decreases from ~ 10–20 km in the northern part to ~ 5 km in the southern part with the anomalously low values ~ 0–5 km in the central segment of the ridge. They explained that the lack of correlation between the elastic thickness and the lithospheric age implies differences in thermo-mechanical setting of the crust and the underlying mantle along different portions of the Ninety-East Ridge, implying their different geological evolution (see also *Craig and Copley, 2014*). They suggested that the anomalously low strength and a deeper Moho ($\sim$22 km) in its central part are attributed to the interaction of a hotspot with the Wharton spreading ridge that caused a significant thermal rejuvenation and hence weakening of the lithosphere. They also stipulated that a higher mechanical strength in the northern part of the ridge might corroborate the idea of off-ridge emplacement and a relatively large plate motion at the time of volcanism. A weak strength in the southern part, on the other hand, suggests that the lithosphere was younger at the time of volcanism. Consequently, this supports the hypothesis that the southern part of the ridge was emplaced on the edge of the Indian plate.

According to our result, the elastic thickness beneath the western continental margin of India is $\sim$26–41 km, with a slight decrease under the Chagos-Laccadive Plateau and the Arabian Basin ($T_e \sim$ 23–35 km). We also detected a weak lithosphere beneath Madagascar ($T_e \sim$ 15–30 km). Furthermore, our result shows that the elastic thickness beneath the Mascarene Plateau is $\sim$30 km, with local minima at the Réunion and Mauritius hotspots and an additional localized lithospheric weakening ($T_e <$ 15 km) beneath Seychelles. *Chaubey et al. (2008)* conducted the admittance analysis of gravity and bathymetric data along 12 profiles. Their analysis indicates the existence of a weak lithosphere ($T_e \sim$ 2–3 km) across the Laccadive Ridge that could be explained by a local compensation of stretched continental lithosphere. *Kunnummal and Anand (2022)* reported the elastic thickness within 6.5–16.5 km along the Greater Maldive Ridge, based on a flexural model, with lower values ($T_e \sim$ 7–9 km) under the Maldive Ridge and slightly higher values beneath the Deep Sea Channel ($T_e >$ 10 km). *Ratheesh Kumar et al. (2015)* reported a very low strength beneath the Arabian Sea and the Laccadive Ridge ($T_e <$ 3 km), in contrast to higher values of the elastic thickness (up to 20 km) along the western continental margin of India. They also detected relatively low values (up to 20 km) under most of Madagascar, Reunion, and Mauritius as well as the existence of a very weal lithosphere ($T_e <$ 5 km) beneath the east coast of

Madagascar. *Chand and Subrahmanyam (2003)* reported a higher strength ($T_e \sim 8$–15 km) in the western continental margin of India. Similarly, *Dev et al. (2012)* detected values of the elastic thickness there varying between 5 and 10 km. *Chand and Subrahmanyam (2003)* also reported values of the elastic thickness between 10 and 13 km for the eastern continental margin of Madagascar. Our estimate generally agrees better with values reported by *Chand and Subrahmanyam (2003).* According to *Tiwari et al. (2007)*, the elastic thickness beneath the Réunion and Mauritius is ~ 30 km, but later *Trivedi et al. (2012)* suggested lower strength ($T_e \sim 20$ km). Our values for these two hotspots are < 15 km. *Trivedi et al. (2012)* also reported small values of the elastic thickness ($T_e \sim 1$–6 km) along the Chagos-Laccadives Ridge, arguing its proximity to a spreading ridge at the time of its formation. Their numerical findings also indicate spatial correlation of the elastic thickness with the ocean-floor age along the Mascarene Plateau, with an increasing strength from north ($T_e \sim 4$ km) to south ($T_e \sim 20$ km). Our result, based on a thermal state of the oceanic lithosphere, exhibits a prevailing westward trending of increasing values ($T_e \sim 28$–35 km) that actually better agree with a prevailing orientation of the ocean-floor spreading.

Grevemeyer et al. (2001) reported the elastic thickness of 20–25 km beneath volcanic islands of the Kerguelen Plateau. Our result indicates a weak lithosphere at the hotspot location ($T_e < 15$ km), but a much large strength beneath the South Kerguelen Plateau, with maxima of the elastic thickness up to $\sim$130 km. We explain such large values by the fact that the South Kerguelen Plateau is formed by old, stable fragments of the continental crust, characterized also by a large crustal thickness.

5.2. Sri Lanka and India

We detected a weak strength of the lithosphere ($T_e < 24$–35 km) beneath Sri Lanka. Our result is in a good agreement with estimates 24–36 km and 28–34 km reported by *Ratheesh Kumar et al. (2020)* and *Prasanna et al. (2014)*, respectively. Both collectives of authors also provided estimates for South India between 30 and 40 km. According to our result, these low values of the elastic thickness ($T_e \sim 20$–40 km) extend beneath South India and the Deccan Traps. In contrast, we see a partially increasing strength of the lithosphere beneath the Dharwar-Bastar ($T_e \sim 35$–60 km) and Singbhum Cratons ($T_e \sim 35$–70 km), both forming Archean cratons of Indian Peninsula. *Rajesh and Mishra (2004)* reported lower values ($T_e \sim 12$–26 km) for Archean cratons and Proterozoic mobile belts of the Indian subcontinent based on a robust coherence multi-taper spectral analysis. Further north, our result shows a significantly increasing lithospheric strength under the Aravalli and Bundelkhand Cratons, with the elastic thickness exceeding 180 km. The Central Indian Tectonic Zone is to some extent manifested in our elastic thickness map by the contrast between a weak lithospheric strength to the south (including the Deccan Traps) and a much higher strength of the Archean cratons to the north. Our result for the Deccan Traps ($T_e \sim 25$–40 km) differs from published results. *Tiwari and Mishra (1999)* reported the elastic thickness of 10–15 km, and *Jordan and Watts (2005)* provided values less than 5 km.

The first attempts to estimate the elastic thickness of the Indian subcontinent can be attributed to *Lyon-Caen and Molnar (1985)* and *Karner and Watts (1983)*. They applied a forward modelling technique and used the Bouguer gravity and topographic data. According to their analyses, the elastic thickness beneath the Ganges Basin is 80–110 km. Our result there varies significantly ($T_e \sim 30$–100 km) reflecting on a particular tectonic setting. *McKenzie and Fairhead (1997)* applied the admittance analysis of the free-air gravity and topographic data. They reported values less than 24 km. By using a multi-taper spectral analysis, *Rajesh et al. (2003)* characterized relative variations of the elastic thickness along a continental tectonic collision of the Indian and Eurasian plates. *Jordan and Watts (2005)* used both, the forward and inverse flexural and gravity modelling and obtained values between 0 and 125 km along this collision zone. Our result for the eastern part of this tectonic margin is $T_e \sim 15$–110 km. *Hetényi et al. (2006)* suggested that the continental elastic thickness of the Indian plate decreases northwards from 60–80 to 20–30 km as it is bended underneath Himalaya and Tibet, due to a thermal and flexural weakening. This trend does not agree with our finding. Our result exhibit a generally increasing strength northwards beneath the Indian Peninsula. A similar trend was reported before by *Ratheesh Kumar et al. (2014)* who applied the isotropic fan-wavelet method to study the lithospheric strength of the Indian Shield. They explained that a thinned, attenuated lithosphere beneath Peninsular India is the reason for its mechanically weak strength ($T_e < 30$ km), where a decoupled crust–mantle rheology under different loading structures may explain prominently low strength of the lithosphere. They further stated that the old, stable parts lithospheric structures of the Central Indian Tectonic Zone, the Bastar Craton, and the northern Eastern Ghats Mobile Belt have higher strength ($T_e \sim 40$–50 km), providing the explanation that these formations were not affected by any major tectono-thermal events after cratonic stabilization. They also reported a large anomaly ($T_e \sim 60$–85 km) in Northwest Himalaya including the northern Aravalli and Bundelkhand Cratons.

5.3. Arabian Peninsula and Iran

Our estimates of the elastic thickness within the Arabian Plate revealed striking contrast between the Arabian platform ($T_e \sim 15$–50 km) and shield ($T_e \sim 35$–95 km) regions. This finding agrees with previously published results (*Audet and Bürgmann, 2011; Tesauro et al., 2013; Chen et al., 2015; Tesauro et al., 2018; Eshagh and Pitoňák, 2019; Gedamu et al., 2021*). *Audet and Bürgmann (2011)* and *Tesauro et al. (2013)* used the inverse cross-spectral and forward rheological approaches. They estimated that the elastic thickness in East Arabia is ~ 40–60 km. *Chen et al. (2015)* inferred values ∼50 km in East Arabia and 10–30 km in West Arabia. *Tesauro et al. (2018)* incorporated the effects of temperature, composition, and strain rate and obtained values ~ 60–80 km in East Arabia. Values in the range of 40–70 km for the eastern Arabian platform were reported by *Eshagh and Pitoňák (2019).* In the most recent study, *Ismaiel et al. (2023)* obtained values ranging from 10 to 50 km, with a minimum strength of the lithosphere ($T_e < 20$ km) in the south part of East Arabia and an increasing strength ($T_e \sim 30$–45 km) in the northeastern regions of Saudi Arabia. These estimates roughly agree with our result, confirming that a significant strength of the Arabian Platform differs considerably from an apparently weak lithosphere of the Arabian Shield ($T_e < 40$ km). Studies suggest that the origin of the Arabian Shield was formed together with the Nubian Shield during the East African Orogenesis, prior to Gondwana breakup (e.g., *Johnson and Woldehaimanot, 2003*). A separation of the Arabian-Nubian Shield into two segments that began in the Eocene is attributed to divergent tectonism along the Red Sea-Gulf Rift System (e.g., *McGuire and Bohannon, 1989).* A low strength of the Arabian Shield might be explained by findings of *Park et al. (2008).* They modelled a shear-wave velocity structure of shallow upper mantle beneath the Arabian Shield by inverting the Rayleigh wave phase velocity measurements. Their model revealed a broad low-velocity region down to depths ∼150 km in the mantle across the shield and a narrower low-velocity region at depths 150 km localized along the Red Sea coast and Makkah-Madinah-Nafud volcanic line. This velocity reduction in the upper mantle corresponds to a temperature anomaly of 250–330 K. According to their interpretations, the mantle structure is possibly controlled by an upwelling of warm mantle rocks originating in the lower mantle under Africa that crosses through the mantle transition zone beneath Ethiopia and moves to the north and northwest under the eastern margin of the Red Sea and the Arabian Shield.

According to *Eshagh et al. (2020)*, seismically and volcanically active convergent tectonic margins of the Zagros and Kopeh Dagh Fold and Thrust Belts spreading further along the Makran Accretionary Complex have a low lithospheric strength ($T_e < 30$ km). These finding agree with our result. This weak lithosphere is in a striking contrast to much stiffer lithosphere beneath most of the Central Iranian Block, where maxima of the elastic thickness locally reach ∼70 km within the Tabas micro-block.

5.4. East Africa

The extended continental crust of East Africa is characterized by a weak lithosphere ($T_e < 30$ km). A weak lithosphere is also detected under the Afar hotspot ($T_e < 15$ km) and the northern and central segments of the East-African Rift System ($T_e < 25$ km). In Central Africa, the elastic thickness increases to ∼150 km or more beneath the Archean cratons. Our result relatively closely agrees with the elastic thickness map of Africa presented by *Pérez-Gussinye et al. (2009a)*. Our result also supports the findings by *Gedamu et al. (2021)*. They reported values consistent with a significant lithospheric strength present in cratonic formations, with the maximum elastic thickness of the Sudan and Tanzanian Cratons, while low values prevail along tectonically active locations, including the Afar and the Main Ethiopian Rift Valley.

5.5. Southeast Asia

We detected a weak lithosphere (T_e∼20–40 km) along the West Burma Block in constant to considerable elastic thickness variations (T_e ∼ 30–120 km) along of the Sibumasu Block. The Indochina block and the west part of the East Malaya Block are manifested by a high lithospheric strength ($T_e \sim 70$–110 km). Borneo is characterized by mild changes in the elastic thickness ($T_e \sim 20$–40 km). These estimates roughly agree with results presented by *Shi et al. (2017)*.

According to our result, the elastic thickness along the Java-Sunda oceanic subduction zone varies quite substantially, from 16 to ~ 140 km under some segments of accretionary wedges. This relatively complex pattern could be explained by several factors that are attributed to a stress and thermal distribution, with a cold oceanic lithosphere sinking beneath the overriding plate into the mantle causing volcanism and deformations on the side of continental lithosphere (cf. *Raghuram et al., 2018*). The flexural bending of subducted lithosphere could be attributed mainly to a vertical end load and bending moment of the negative buoyancy force acting on a plate, the slab pull (e.g., *Watts and Talwani, 1974*) along with other tectonic forces, such as shearing along an intraplate margin and a horizontal forcing across the margin. The response of the oceanic lithosphere to these forces can be observed in the seafloor bulge of the plate (e.g., *Walcott, 1970*) near the trench, a pervasive normal faulting near the outer-arc trench (e.g., *Ranero et al., 2005*) along with an inferred lithospheric weakening that results in a decreasing elastic thickness of the plate closer to the trench (e.g., *Bassett and Watts, 2015*). It is commonly assumed that the bending, deformation, and further weakening of the oceanic lithosphere respond mostly to the amount of slab pull attached, while shear along the margin and horizontal forces are negligible (e.g., *Forsyth and Uyeda, 1975; Levitt and Sandwell, 1995*). A relatively complex pattern of lithospheric strength was reported also by *Shi et al. (2017)*. According to their results, the incoming oceanic plate becomes weaker along the Sunda Trench when approaching the trench axis. They suggested a possible reason by the development of bending faults and plate bending before subduction (*Burov, 2011*). However, since the incoming plate is topographically rough, with oceanic plateaus and seamounts, the elastic thickness pattern in the subduction system, particularly in the southern Sumatra Trench and the Java Trench, is complicated by the approach and collision of oceanic basement relief with the fore-arc regions. *Nair et al. (2011)* obtained different numerical findings. They presented a uniformly weak lithosphere beneath the subducting oceanic plate in the

Indonesian continental margin. Their results reveal a fluctuating flexural anisotropy that correlates with a maximum horizontal stress orientation, which they attributed to the coherent and incoherent deformations of a truly anisotropic plate margin (see also *Ratheesh Kumar et al., 2013*).

5.6. West Australia

The lithospheric strength in West Australia is manifested by maxima within the Pilibara and Yilgarm Cratons. These cratons are clearly separated from the Arunta Craton in central-west Australia by smaller values of the elastic thickness along the Paterson and Musgrave orogenic belts. Our findings more or less agree with the results by *Zuber et al. (1989).* They stated that continental regions of different origin and tectonic history could be generally characterized by an increasing strength (i.e., elastic thickness) with age after their lithospheric stabilization. According to their result, the Precambrian shields situated in West, North, and South Australia have the elastic thickness of the order of 100 km. The lithospheric strength beneath the Phanerozoic Interior Lowlands lessens ($T_e \sim 30$–80 km) and under the Eastern Highlands further weakens ($T_e \sim 15$–35 km). Our estimates differ from the result presented by *Swain and Kirby (2006).* They presented a gradually strengthening lithosphere from coastal areas towards inland, but without reflecting actual geological configuration of this continent.

5.7. Relationship between the elastic thickness, gravity, and crustal geometry

To inspect a possible link between the lithospheric strength and gravity field (i.e., the free-air and Bouguer gravity disturbances) as well as crustal geometry (i.e., the Moho depth and topographic/bathymetric relief), we plotted these values along two profiles. The first profile (Fig. 7a) coincides with the equator. This profile intercepts the continental divergent tectonic margin (i.e., the East-African Rift System), the oceanic divergent tectonic margin (i.e., the Carlsberg Ridge), the igneous province (i.e., the Chagos-Laccadive Plateau), the meridional aseismic ridge (i.e., Ninety-East Ridge), and the oceanic subduction zone (i.e., the Java-Sunda Trench). We further selected the meridional profile of 90° E longitude (Fig. 7b). This profile intersects the oceanic divergent tectonic margin (i.e., the Southeast Indian Ridge), the aseismic ridge (i.e. the Broken Ridge), the oceanic subduction zone (i.e., the

Java-Sunda Trench) including the volcanic arc, and the active continental convergent margin and the orogeny (i.e., the Himalaya).

A high spatial correlation between the Bouguer gravity disturbances and the Moho geometry is particularly manifested under the continental crust. A spatial correlation between the free-air gravity disturbances and

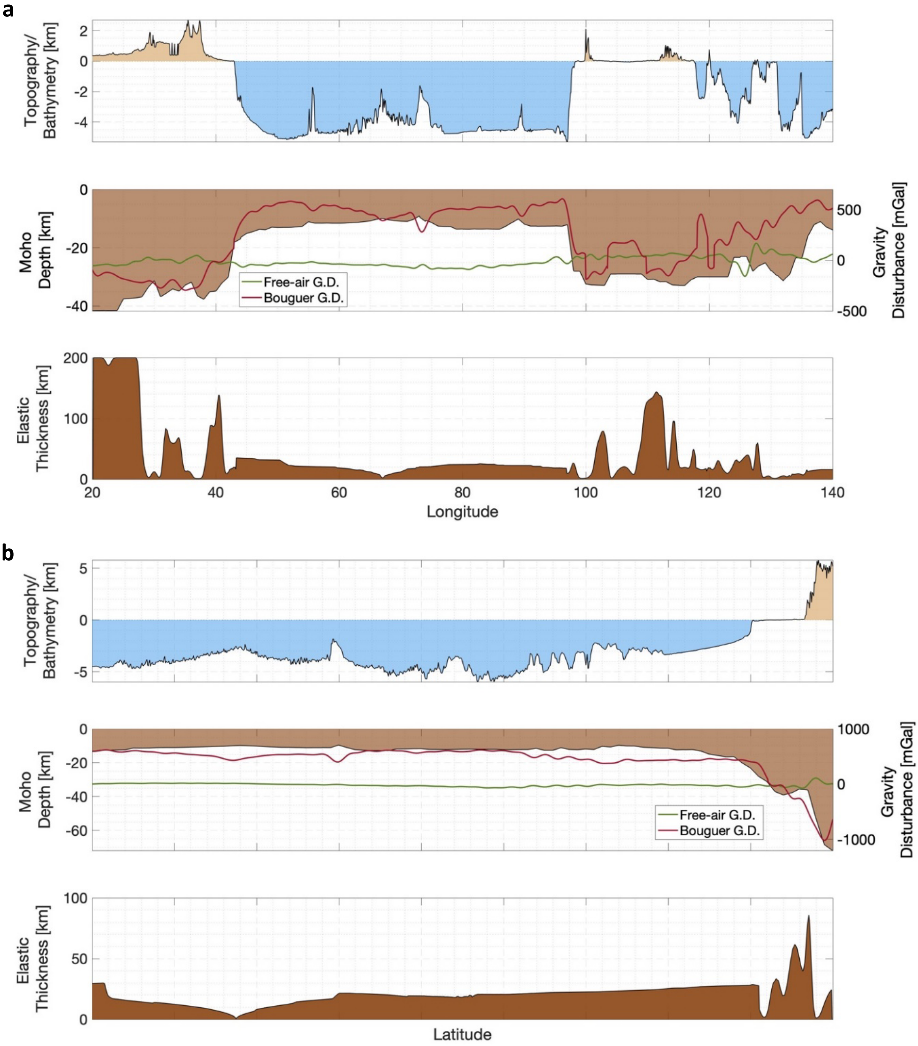

Fig. 7. The effective elastic thickness profiles: (a) along the equator, and (b) along the meridian of 90° E latitude.

the topographic/bathymetric relief is much less pronounced. Although an overall spatial correlation between the elastic thickness and the topographic/bathymetric relief is not clearly manifested, we could partially recognize a similar trend between an increasing elastic thickness and a gradual ocean-floor deepening on both sides of mid-oceanic rifts. Such trend in the elastic thickness was explained by an increasing strength of the oceanic lithosphere due to its conductive cooling. An increasing ocean-floor depth is attributed to an isostatic rebalance of the oceanic lithosphere. In this respect, we could also find a link between an increasing trend of the elastic thickness and a decreasing trend (in absolute sense) of the Bouguer gravity disturbances on both sides of mid-oceanic rift zones.

A possible spatial correlation between the elastic thickness and a Moho geometry is not obvious. However, a larger T_e can be observed in the relative maxima of the Moho depth in the continental lithosphere (in Fig. 7 there are three maxima between 20° and 40°). T_e is also greater when the Moho is deeper and smaller in the centre (ridge) along the oceanic portion. Moreover, between 100° and 140° different Moho maxima and minima coincides with maxima and minima of T_e.

6. Summary and concluding remarks

We have estimated the effective elastic thickness beneath the Indian Ocean and surrounding continental regions. We applied two methods that are capable to better distinguish between different properties that mainly govern the strength of the oceanic and continental lithosphere. Hence, the strength of the oceanic lithosphere that is mainly controlled by its thermal state was computed using a mathematical model that defines the elastic thickness as a function of age and temperature of the oceanic lithosphere. This model reflects the fact that a conductive cooling of the oceanic lithosphere increases its strength in time. For the continental lithosphere, we applied the method developed by *Eshagh (2018)* that combines the Vening Meinesz-Moritz regional isostatic principle with the isostatic flexural model formulated based on solving a flexural differential equation for a thin elastic shell. This method takes into consideration rheological properties of the continental lithosphere more realistically than methods based a cross-spectral analysis (such as the admittance or coherence) of gravity and topographic data or gravimetric isostatic models. This was particularly achieved by taking into consideration the lithospheric properties (i.e., the Young modulus and the Poisson ratio) and density structure that allow describing the response of the lithosphere on a load and stresses more realistically. Principle of this method is that the elastic thickness is estimated in such a way that the flexural Moho can approximate the gravimetric Moho depth. In other words, the norm of their difference is minimized, but this minimum may not exist. Another important issue is that the results should be filtered in spatial domain to remove or reduce the zero and large values of the estimated elastic thickness which are results of non-existence the minima.

The applied model for modelling the oceanic elastic thickness is a function of upper mantle temperature and the age of lithosphere. There are available global models for these parameters, but since they are of global nature, lacking details, the estimated elastic thickness in our study has a limited spatial resolution. Nevertheless, overall pattern of the elastic thickness variations provided a relatively comprehensive information about the lithospheric strength. According to our result, the elastic thickness relatively closely mimics tectonic and geological configuration of the Indian Ocean. Minima of the elastic thickness indicate a weak lithosphere along active divergent tectonic margins of mid-oceanic ridges. A localized weak lithosphere was also detected at hotspots. The elastic thickness of the oceanic lithosphere gradually increases with its age, reflecting the fact that a thermal state mainly controls its strength. The isostatic rebalance of the oceanic lithosphere, on the other hand, very likely does not substantially modify the lithospheric strength. The continental lithosphere is characterized by much large variations of the elastic thickness, with a weak lithosphere beneath the extended continental crust, igneous provinces, and continental rift systems. Maxima prevail within old, stable cratonic formations, while active orogenic formations have typically a much weaker strength.

We argue that existing studies of the elastic thickness of volcanic islands, seamounts, igneous oceanic provinces, and aseismic ridges based on applying a cross-spectral analysis (i.e. admittance or coherence) or isostatic models are not fully appropriate due to disregarding a thermal state of these volcanic formations, especially of younger geological age. These models likely also underestimate a mechanical strength of the old oceanic lithosphere. The method applied in this study takes into consideration a thermal state of the oceanic lithosphere but disregards an isostatic state of volcanic formations (e.g., *Cazenave et al., 1980*). Optimally both, the thermal and isostatic states of volcanic formations should be considered, but such model has not yet been developed (due to its theoretical complexity) and validated.

Data availability statement. Data presented in this research are available upon request.

References

Artemjev M. E., Kaban M. K., 1991: Isostatic processes and intracontinental orogenesis. J. Geodyn., **13**, 1, 77–86, doi: 10.1016/0264-3707(91)90031-9.

Ashalatha B., Subrahmanyam C., Singh R. N., 1991: Origin and compensation of Chagos-Laccadive Ridge, Indian Ocean, from admittance analysis of gravity and bathymetry data. Earth Planet. Sci. Lett., **105**, 1-3, 47–54, doi: 10.1016/0012-821X(91)90119-3.

Audet P., Mareschal J.-C., 2004: Variations in elastic thickness in the Canadian Shield. Earth Planet. Sci. Lett., **226**, 1-2, 17–31, doi: 10.1016/j.epsl.2004.07.035.

Audet P., Bürgmann R., 2011: Dominant role of tectonic inheritance in supercontinent cycles. Nat. Geosci., **4**, 3, 184–187, doi: 10.1038/ngeo1080.

Bandopadhyay P. C., Carter A., 2017: Geological framework of the Andaman–Nicobar Islands. In: Bandopadhyay P. C., Carter A. (Eds.): The Andaman–Nicobar Accretionary Ridge: Geology, Tectonics and Hazards. Memoirs, **47**, Geological Society, London, pp. 75–93., doi: 10.1144/M47.6.

Bansal A. R., Fairhead J. D., Green C. M., Fletcher K. M. U., 2005: Revised gravity for offshore India and the isostatic compensation of submarine features. Tectonophysics, **404**, 1-2, 1–22, doi: 10.1016/j.tecto.2005.03.017.

Bassett D., Watts A. B., 2015: Gravity anomalies, crustal structure, and seismicity at subduction zones: 1. Seafloor roughness and subducting relief. Geochem. Geophys. Geosyst., **16**, 5, 1508–1540, doi: 10.1002/2014GC005685.

Braitenberg C., Ebbing J., Götze H.-J., 2002: Inverse modelling of elastic thickness by convolution method – the Eastern Alps as a case example. Earth Planet. Sci. Lett., **202**, 2, 387–404, doi: 10.1016/S0012-821X(02)00793-8.

Brockmann J. M., Schubert T., Mayer-Gürr T., Schuh W.-D., 2019: The Earth's gravity field as seen by the GOCE satellite – an improved sixth release derived with the time-wise approach (GO_CONS_GCF_2_TIM_R6). GFZ Data Services, doi: 10.5880/ICGEM.2019.003.

Burov E. B., Diament M., 1995: The effective elastic thickness (T_e) of continental lithosphere: What does it really mean? J. Geophys. Res. Solid Earth, **100**, B3, 3905–3927, doi: 10.1029/94JB02770.

Burov E., Diament M., 1996: Isostasy, equivalent elastic thickness, and inelastic rheology of continents and oceans. Geology, **24**, 5, 419–422, doi: 10.1130/0091-7613(1996)024<0419:IEETAI>2.3.CO;2.

Burov E. B., 2011: Rheology and strength of the lithosphere. Mar. Pet. Geol., **28**, 8, 1402–1443, doi: 10.1016/j.marpetgeo.2011.05.008.

Calmant S., Francheteau J., Cazenave A., 1990: Elastic layer thickening with age of the oceanic lithosphere: a tool for prediction of the age of volcanoes or oceanic crust. Geophys. J. Int., **100**, 1, 59–67, doi: 10.1111/j.1365-246X.1990.tb04567.x.

Carslaw H. S., Jaeger J. C., 1959: Conduction of heat in solid (2nd ed.). Clarendon Press, Oxford.

Cazenave A., Lago B., Dominh K., Lambeck K., 1980: On the response of the ocean lithosphere to sea-mount loads from *Geos 3* satellite radar altimeter observations. Geophys. J. Int., **63**, 1, 233–252, doi: 10.1111/j.1365-246X.1980.tb02618.x.

Chand S., Subrahmanyam C., 2003: Rifting between India and Madagascar – mechanism and isostasy. Earth Planet. Sci. Lett., **210**, 1-2, 317–332, doi: 10.1016/S0012-821X(03)00094-3.

Chaubey A. K., Srinivas K., Ashalatha B., Rao D. G., 2008: Isostatic response of the Laccadive Ridge from admittance analysis of gravity and bathymetry data. J. Geodyn., **46**, 1-2, 10–20, doi: 10.1016/j.jog.2008.03.001.

Chen W., Tenzer R., Gu X., 2014: Sediment stripping correction to marine gravity data. Mar. Geod., **37**, 4, 419–439, doi: 10.1080/01490419.2014.932870.

Chen B., Kaban M. K., El Khrepy S., Al-Arifi N., 2015: Effective elastic thickness of the Arabian plate: Weak shield versus strong platform. Geophys. Res. Lett., **42**, 9, 3298–3304, doi: 10.1002/2015GL063725.

Chen W., Tenzer R., 2020: Reformulation of Parker–Oldenburg's method for Earth's spherical approximation. Geophys. J. Int., **222**, 2, 1046–1073, doi: 10.1093/gji/ggaa200.

Cloetingh S., Burov E. B., 1996: Thermomechanical structure of European continental lithosphere: constraints from rheological profiles and EET estimates. Geophys. J. Int., **124**, 3, 695–723, doi: 10.1111/j.1365-246X.1996.tb05633.x.

Coffin M. F., Pringle M. S., Duncan R. A., Gladczenko T. P., Storey M., Müller R. D., Gahagan L. A., 2002: Kerguelen hotspot magma output since 130 Ma. J. Petrol., **43**, 7, 1121–1137, doi: 10.1093/petrology/43.7.1121.

Craig T. J., Copley A., 2014: An explanation for the age independence of oceanic elastic thickness estimates from flexural profiles at subduction zones, and implications for continental rheology. Earth Planet. Sci. Lett., **392**, 207–216, doi: 10.1016/j.epsl.2014.02.027.

Dev S. V., Radhakrishna M., Chand S., Subrahmanyam C., 2012: Gravity anomalies, crustal structure and rift tectonics at the Konkan and Kerala basins, western continental margin of India. J. Earth Syst. Sci., **121**, 3, 813–822, doi: 10.1007/s12040-012-0186-6.

Doucouré C. M., de Wit M. J., Mushayandebvu M. F., 1996: Effective elastic thickness of the continental lithosphere in South Africa. J. Geophys. Res. Solid Earth, **101**, B5, 11291–11303, doi: 10.1029/95JB03718.

Eshagh M., 2016a: On Vening Meinesz-Moritz and flexural theories of isostasy and their comparison over Tibet Plateau. J. Geod. Sci., **6**, 1, 139–151, doi: 10.1515/JOGS-2016-0013.

Eshagh M., 2016b: A theoretical discussion on Vening Meinesz-Moritz inverse problem of isostasy. Geophys. J. Int., **207**, 3, 1420–1431, doi: 10.1093/gji/ggw344.

Eshagh M., 2017: On the approximations in formulation of the Vening Meinesz–Moritz theory of isostasy. Geophys. J. Int., **210**, 1, 500–508, doi: 10.1093/gji/ggx179.

Eshagh M., 2018: Elastic thickness determination based on Vening Meinesz-Moritz and flexural theories of isostasy. Geophys. J. Int., **213**, 3, 1682–1692, doi: 10.1093/gji/ggy075.

Eshagh M., Pitoňák M., 2019: Elastic Thickness Determination from on-orbit GOCE Data and CRUST1.0. Pure Appl. Geophys., **176**, 2, 685–696, doi: 10.1007/s00024-018-2018-3.

Eshagh M., Pitoňák M., Tenzer R., 2019: Lithosperic elastic thickness estimates in central Eurasia. Terr. Atmos. Ocean. Sci., **30**, 1, 73–84, doi: 10.3319/TAO.2018.09.28.02.

Eshagh M., Tenzer R., Eshagh M., 2020: Elastic thickness of the Iranian lithosphere from gravity and seismic data. Tectonophysics, **774**, 228186, doi: 10.1016/j.tecto.2019.228186.

Eshagh M., Tenzer R., 2021: The temporal viscoelastic model of flexural isostasy for estimating the elastic thickness of the lithosphere. Geophys. J. Int., **227**, 3, 1700–1714, doi: 10.1093/gji/ggab292.

Filmer P. E., McNutt M. K., Wolfe C. J., 1993: Elastic thickness of the lithosphere in the Marquesas and Society Islands. J. Geophys. Res. Solid Earth, **98**, B11, 19565–19577, doi: 10.1029/93JB01720.

Flück P., Hyndman R. D., Lowe C., 2003: Effective elastic thickness T_e of the lithosphere in western Canada. J. Geophys. Res. Solid Earth, **108**, B9, 2430, doi: 10.1029/2002JB002201.

Forsberg R., Olesen A. V., Ferraccioli F., Jordan T., Corr H., Matsuoka K., 2017: Polargap 2015/2016: Filling the GOCE Polar Gap in Antarctica and ASIRAS flight around South Pole. Final Report, ESA, available at https://earth.esa.int/eogateway/documents/20142/37627/PolarGap-2015-2016-final-report.pdf, accesed 25 June 2025.

Forsyth D., Uyeda S., 1975: On the relative importance of the driving forces of plate motion. Geophys. J. Int., **43**, 1, 163–200, doi: 10.1111/j.1365-246X.1975.tb00631.x.

Forsyth D. W., 1985: Subsurface loading and estimates of the flexural rigidity of continental lithosphere. J. Geophys. Res. Solid Earth, **90**, B14, 12623–12632, doi: 10.1029/JB090iB14p12623.

Forsyth D. W., Ehrenbard R. L., Chapin S., 1987: Anomalous upper mantle beneath the Australian-Antarctic discordance. Earth Planet. Sci. Lett., **84**, 4, 471–478, doi: 10.1016/0012-821X(87)90011-2.

French S. W., Romanowicz B., 2015: Broad plumes rooted at the base of the Earth's mantle beneath major hotspots. Nature, **525**, 95–99, doi: 10.1038/nature14876.

Galán R. A., Casallas I. F., 2010: Determination of effective elastic thickness of the Colombian Andes using satellite-derived gravity data. Earth Sci. Res. J., **14**, 1, 7–16, doi: 10.15446/esrj.v14n1.21089.

Gedamu A. A., Eshagh M., Bedada T. B., 2021: Effects of mantle dynamics on estimating effective elastic thickness of the lithosphere. J. Afr. Earth Sci., **183**, 104318, doi: 10.1016/j.jafrearsci.2021.104318.

Gladkikh V., Tenzer R., 2012: A mathematical model of the global ocean saltwater density distribution. Pure Appl. Geophys., **169**, 1-2, 249–257, doi: 10.1007/s00024-011-0275-5.

Gómez-Ortiz D., Tejero R., Ruiz J., Babín-Vich R., González-Casado J. M., 2005: Estimating the effective elastic thickness of the lithosphere of the Iberian Peninsula based on multitaper spectral analysis. Geophys. J. Int., **160**, 2, 729–735, doi: 10.1111/j.1365-246X.2004.02499.x.

Grevemeyer I., Weigel W., Schüssler S., Avedik F., 2001: Crustal and upper mantle seismic structure and lithospheric flexure along the Society Island hotspot chain. Geophys. J. Int., **147**, 1, 123–140, doi: 10.1046/j.0956-540x.2001.01521.x.

Gu X., Tenzer R., Gladkikh V., 2014: Empirical models of the ocean-sediment and marine sediment-bedrock density contrasts. Geosci. J., **18**, 4, 439–447, doi: 10.1007/s12303-014-0015-9.

Heiskanen W. A., Moritz H., 1967: Physical Geodesy. W. H. Freeman and Co., San Francisco-London.

Hetényi G., Cattin R., Vergne J., Nábělek J., 2006: The effective elastic thickness of the India Plate from receiver function imaging, gravity anomalies and thermomechanical modelling. Geophys. J. Int., **167**, 3, 1106–1118, doi: 10.1111/j.1365-246X.2006.03198.x.

Hirt C., Rexer M., 2015: Earth2014: 1 arc-min shape, topography, bedrock and ice-sheet models – Available as gridded data and degree-10,800 spherical harmonics. Int. J. Appl. Earth Obs. Geoinf., **39**, 103–112, doi: 10.1016/j.jag.2015.03.001.

Hyndman R. D., Currie C. A., Mazzotti S. P., 2005: Subduction zone backarcs, mobile belts, and orogenic heat. GSA Today, **15**, 2, 4–10, doi: 10:1130/1052-5173(2005)015<4:SZBMBA>2.0.CO;2.

Ismaiel M., Ali M. Y., Watts A. B., Barkat B., 2023: Spatial variations of effective elastic thickness of Eastern Arabia: Implications for lithospheric weakening in the Oman-UAE mountain belt. Tectonophysics, **863**, 229995, doi: 10.1016/j.tecto.2023.229995.

Jackson J., Haines J., Holt W., 1995: The accommodation of Arabia-Eurasia plate convergence in Iran. J. Geophys. Res. Solid Earth, **100**, B8, 15205–15219, doi: 10.1029/95JB01294.

Johnson P. R., Woldehaimanot B., 2003: Development of the Arabian-Nubian Shield: perspectives on accretion and deformation in the northern East African Orogen and the assembly of Gondwana. Geol. Soc. Spec. Publ., **206**, 1, 289–325, doi: 10.1144/GSL.SP.2003.206.01.15.

Jordan T. H., 1979: Mineralogies, densities and seismic velocities of garnet lherzolites and their geophysical implications. In: Boyd F. R., Meyer H. O. A. (Eds.): The mantle sample: Inclusion in kimberlites and other volcanics, **16**, 1–14, AGU, doi: 10.1029/SP016p0001.

Jordan T. A., Watts A. B., 2005: Gravity anomalies, flexure and the elastic thickness structure of the India–Eurasia collisional system. Earth Planet. Sci. Lett., **236**, 3-4, 732–750, doi: 10.1016/j.epsl.2005.05.036.

Karner G. D., Watts A. B., 1983: Gravity anomalies and flexure of the lithosphere at mountain ranges. J. Geophys. Res. Solid Earth, **88**, B12, 10449–10477, doi: 10.1029/JB088iB12p10449.

Kirby J. F., 2014: Estimation of the effective elastic thickness of the lithosphere using inverse spectral methods: The state of the art. Tectonophysics, **631**, 87–116, doi: 10.1016/j.tecto.2014.04.021.

Kunnummal P., Anand S. P., 2022: Crustal structure and tectonic evolution of Greater Maldive Ridge, Western Indian Ocean, in the context of plume-ridge interaction. Gondwana Res., **106**, 142–163, doi: 10.1016/j.gr.2022.01.006.

Laske G., Masters G., Ma Z., Pasyanos M., 2013: Update on CRUST1.0 – A 1-degree global model of Earth's crust. In: Geophys. Res. Abstr., **15**, EGU2013-2658.

Levitt D. A., Sandwell D. T., 1995: Lithospheric bending at subduction zones based on depth soundings and satellite gravity. J. Geophys. Res. Solid Earth, **100**, B1, 379–400, doi: 10.1029/94JB02468.

Lowry A. R., Smith R. B., 1995: Strength and rheology of the western U.S. Cordillera. J. Geophys. Res. Solid Earth, **100**, B9, 17947–17963, doi: 10.1029/95JB00747.

Lyon-Caen H., Molnar P., 1985: Gravity anomalies, flexure of the Indian Plate, and the structure, support and evolution of the Himalaya and Ganga Basin. Tectonics, **4**, 6, 513–538, doi: 10.1029/TC004i006p00513.

McGovern P. J., Solomon S. C., Smith D. E., Zuber M. T., Simons M., Wieczorek M. A., Phillips R. J., Neumann G. A., Aharonson O., Head J. W., 2002: Localized gravity/topography admittance and correlation spectra on Mars: Implications for regional and global evolution. J. Geophys. Res. Planets, **107**, E12, 19-1–19-25, doi: 10.1029/2002JE001854.

McGuire A. V., Bohannon R. G., 1989: Timing of mantle upwelling: Evidence for a passive origin for the Red Sea rift. J. Geophys. Res. Solid Earth, **94**, B2, 1677–1682, doi: 10.1029/JB094iB02p01677.

McKenzie D., Fairhead D., 1997: Estimates of the effective elastic thickness of the continental lithosphere from Bouguer and free air gravity anomalies. J. Geophys. Res. Solid Earth, **102**, B12, 27523–27552, doi: 10.1029/97JB02481.

McKenzie D., 2003: Estimating T_e in the presence of internal loads. J. Geophys. Res. Solid Earth, **108**, B9, 2438, doi: 10.1029/2002JB001766.

McKenzie D., 2010: The influence of dynamically supported topography on estimates of T_e. Earth Planet. Sci. Lett., **295**, 1-2, 127–138, doi: 10.1016/j.epsl.2010.03.033.

Melluso L., Morra V., 2000: Petrogenesis of Late Cenozoic mafic alkaline rocks of the Nosy Be archipelago (northern Madagascar): relationships with the Comorean magmatism. J. Volcanol. Geotherm. Res., **96**, 1-2, 129–142, doi: 10.1016/S0377-0273(99)00139-0.

Mishra A., Chaubey A. K., Sreejith K. M., Kumar S., 2018: Crustal underplating and effective elastic plate thicknessof the Laxmi Ridge, northern Arabian Sea. Tectonophysics, **744**, 82–92, doi: 10.1016/j.tecto.2018.06.013.

Mishra A., Chaubey A. K., Kumar S., Kumar P. V., Kumar P., Dubey K. M., 2020: Does the Laxmi Ridge continue towards the Laccadive Ridge? New insights from an integrated geophysical study. J. Asian Earth Sci., **201**, 104491, doi: 10.1016/j.jseaes.2020.104491.

Munschy M., Schlich R., 1989: The Rodriguez Triple Junction (Indian Ocean): Structure and evolution for the past one million years. Mar. Geophys. Res., **11**, 1, 1–14, doi: 10.1007/BF00286244.

Müller R. D., Royer J.-Y., Lawver L. A., 1993: Revised plate motions relative to the hotspots from combined Atlantic and Indian Ocean hotspot tracks. Geology, **21**, 3, 275–278, doi: 10.1130/0091-7613(1993)021<0275:RPMRTT>2.3.CO;2.

Müller R. D., Zahirovic S., Williams S. E., Cannon J., Seton M., Bower D. J., Tetley M. G., Heine C., Le Breton E., Liu S., Russell S. H. J., Yang T., Leonard J., Gurnis M., 2019: A global plate model including lithospheric deformation along major rifts and orogens since the Triassic. Tectonics, **38**, 6, 1884–1907, doi: 10.1029/2018TC005462.

Nair R. R., Maji T. K., Maiti T., Kandpal S. Ch., Ratheesh Kumar R. T., Shekhar S., 2011: Multitaper coherence method for appraising the elastic thickness of the Indonesian active continental margin. J. Asian Earth Sci., **40**, 1, 326–333, doi: 10.1016/j.jseaes.2010.06.009.

Ojeda G. Y., Whitman D., 2002: Effect of windowing on lithosphere elastic thickness estimates obtained via the coherence method: Results from northern South America. J. Geophys. Res. Solid Earth, **107**, B11, ETG 3-1–ETG 3-12, doi: 10.1029/2000JB000114.

Park Y., Nyblade A. A., Rodgers A. J., Al-Amri A., 2008: S wave velocity structure of the Arabian Shield upper mantle from Rayleigh wave tomography. Geochem. Geophys. Geosyst., **9**, 7, Q07020, doi: 10.1029/2007GC001895.

Pérez-Gussinyé M., Lowry A. R., Watts A. B., Velicogna I., 2004: On the recovery of effective elastic thickness using spectral methods: Examples from synthetic data and from the Fennoscandian Shield. J. Geophys. Res. Solid Earth, **109**, B10, B10409, doi: 10.1029/2003JB002788.

Pérez-Gussinyé M., Watts A. B., 2005: The long-term strength of Europe and its implications for plate-forming processes. Nature, **436**, 7049, 381–384, doi: 10.1038/nature03854.

Pérez-Gussinyé M., Lowry A. R., Watts A. B., 2007: Effective elastic thickness of South America and its implications for intracontinental deformation. Geochem. Geophys. Geosyst., **8**, 5, Q05009, doi: 10.1029/2006GC001511.

Pérez-Gussinyé M., Metois M., Fernández M., Vergés J., Fullea J., Lowry A. R., 2009a: Effective elastic thickness of Africa and its relationship to other proxies for lithospheric structure and surface tectonics. Earth Planet. Sci. Lett., **287**, 1-2, 152–167, doi: 10.1016/j.epsl.2009.08.004.

Pérez-Gussinyé M., Swain C. J., Kirby J. F., Lowry A. R., 2009b: Spatial variations of the effective elastic thickness, T_e, using multitaper spectral estimation and wavelet methods: Examples from synthetic data and application to South America. Geochem. Geophys. Geosyst., **10**, 4, Q04005, doi: 10.1029/2008GC002229.

Poudjom Djomani Y. H., Nnange J. M., Diament M., Ebinger C. J., Fairhead J. D., 1995: Effective elastic thickness and crustal thickness variations in west central Africa inferred from gravity data. J. Geophys. Res. Solid Earth, **100**, B11, 22047–22070, doi: 10.1029/95JB01149.

Prasanna H. M. I., Chen W., Gómez-Ortiz D., 2014: Geophysical investigation of lithosphere structure beneath Sri Lanka using surface and internal load variations. Pure Appl. Geophys., **171**, 8, 1951–1962, doi: 10.1007/s00024-013-0767-6.

Radha Krishna M., 1996: Isostatic response of the Central Indian Ridge (Western Indian Ocean) based on transfer function analysis of gravity and bathymetry data. Tectonophysics, **257**, 2-4, 137–148, doi: 10.1016/0040-1951(95)00114-x.

Raghuram G., Capitanio F. A., Radhakrishna M., 2018: Flexural analysis along the Sunda Trench: Bending, buckling and plate coupling. Tectonics, **37**, 10, 3524–3544, doi: 10.1029/2017TC004926.

Rajesh R. S., Mishra D. C., 2004: Lithospheric thickness and mechanical strength of the Indian shield. Earth Planet. Sci. Lett., **225**, 3-4, 319–328, doi: 10.1016/j.epsl.2004.06.015.

Rajesh R. S., Stephen J., Mishra D. C., 2003: Isostatic response and anisotropy of the Eastern Himalayan-Tibetan Plateau: A reappraisal using multitaper spectral analysis. Geophys. Res. Lett., **30**, 2, 1060, doi: 10.1029/2002GL016104.

Ranero C. R., Villaseñor A., Morgan J. P., Weinrebe W., 2005: Relationship between bend-faulting at trenches and intermediate-depth seismicity. Geochem. Geophys. Geosyst., **6**, 12, Q12002, doi: 10.1029/2005GC000997.

Ratheesh Kumar R. T., Maji T. K., Nair R. R., 2010: Assessment of flexural analysis applied to the Sumatra-Java subduction zone. J. Earth Syst. Sci., **119**, 5, 717–730, doi: 10.1007/s12040-010-0046-1.

Ratheesh Kumar R. T., Windley B. F., Rajesh V. J., Santosh M., 2013: Elastic thickness structure of the Andaman subduction zone: Implications for convergence of the Ninetyeast Ridge. J. Asian Earth Sci., **78**, 291–300, doi: 10.1016/j.jseaes.2013.01.018.

Ratheesh Kumar R. T., Windley B. F., 2013: Spatial variations of effective elastic thickness over the Ninetyeast Ridge and implications for its structure and tectonic evolution. Tectonophysics, **608**, 847–856, doi: 10.1016/j.tecto.2013.07.034.

Ratheesh Kumar R. T., Windley B. F., Sajeev K., 2014: Tectonic inheritance of the Indian Shield: New insights from its elastic thickness structure. Tectonophysics, **615–616**, 40–52, doi: 10.1016/j.tecto.2013.12.010.

Ratheesh Kumar R. T., Ishwar Kumar C., Windley B. F., Razakamanana T., Nair R. R., Sajeev K., 2015: India–Madagascar paleo-fit based on flexural isostasy of their rifted margins. Gondwana Res., **28**, 2, 581–600, doi: 10.1016/j.gr.2014.06.008.

Ratheesh Kumar R. T., Xiao W., 2018: Effective elastic thickness along the conjugate passive margins of India, Madagascar and Antarctica: A re-evaluation using the Hermite multitaper Bouguer coherence application. J. Asian Earth Sci., **157**, 40–56, doi: 10.1016/j.jseaes.2017.03.019.

Ratheesh Kumar R. T., Dharmapriya P. L., Windley B. F., Xiao W. J., Jeevan U., 2020: The tectonic “umbilical cord” linking India and Sri Lanka and the tale of their failed rift. J. Geophys. Res. Solid Earth, **125**, 5, e2019JB018225, doi: 10.1029/2019JB018225.

Rathnayake S., Tenzer R., Eshagh M., Pitoňák M., 2019: Gravity maps of the lithospheric structure beneath the Indian Ocean. Surv. Geophys., **40**, 5, 1055–1093, doi: 10.1007/s10712-019-09564-6.

Rathnayake S., Tenzer R., Chen W., Eshagh M., Pitoňák M., 2021: Comparison of different methods for a Moho modeling under oceans and marginal seas: A case study for the Indian Ocean. Surv. Geophys., **42**, 4, 839–897, doi: 10.1007/s10712-021-09648-2.

Rao S. G., Radhakrishna M., Sreejith K. M., Krishna K. S., Bull J. M., 2016: Lithosphere structure and upper mantle characteristics below the Bay of Bengal. Geophys. J. Int., **206**, 1, 675–695, doi: 10.1093/gji/ggw162.

Royer J.-Y., Sandwell D. T., 1989: Evolution of the eastern Indian Ocean since the Late Cretaceous: Constraints from Geosat altimetry. J. Geophys. Res. Solid Earth, **94**, B10, 13755–13782, doi: 10.1029/JB094iB10p13755.

Seton M., Müller R. D., Zahirovic S., Williams S., Wright N. M., Cannon J., Whittaker J. M., Matthews K. J., McGirr R., 2020: A global data set of present-day oceanic crustal age and seafloor spreading parameters. Geochem. Geophys. Geosyst., **21**, 10, e2020GC009214, doi: 10.1029/2020GC009214.

Shi X., Kirby J., Yu Ch., Jiménez-Díaz A., Zhao J., 2017: Spatial variations in the effective elastic thickness of the lithosphere in Southeast Asia. Gondwana Res., **42**, 49–62, doi: 10.1016/j.gr.2016.10.005.

Simons F. J., van der Hilst R. D., Zuber M. T., 2003: Spatiospectral localization of isostatic coherence anisotropy in Australia and its relation to seismic anisotropy: Implications for lithospheric deformation. J. Geophys. Res. Solid Earth, **108**, B5, 2250, doi: 10.1029/2001JB000704 .

Sreejith K. M., Krishna K. S., Bansal A. R., 2008: Structure and isostatic compensation of the Comorin Ridge, north central Indian Ocean. Geophys. J. Int., **175**, 2, 729–741, doi: 10.1111/j.1365-246X.2008.03905.x.

Sreejith K. M., Radhakrishna M., Krishna K. S., Majumdar T. J., 2011: Development of the negative gravity anomaly of the 85°E Ridge, northeastern Indian Ocean – A process oriented modelling approach. J. Earth Syst. Sci., **120**, 4, 605–615, doi: 10.1007/s12040-011-0099-9.

Sreejith K. M., Krishna K. S., 2013: Spatial variations in isostatic compensation mechanisms of the Ninetyeast Ridge and their tectonic significance. J. Geophys. Res. Solid Earth, **118**, 10, 5165–5184, doi: 10.1002/jgrb.50383.

Sreejith K. M., Unnikrishnan P., Radhakrishna M., 2019: Isostasy and crustal structure of the Chagos–Laccadive Ridge, Western Indian Ocean: Geodynamic implications. J. Earth Syst. Sci., **128**, 6, 157, doi: 10.1007/s12040-019-1161-2.

Stewart J., Watts A. B., 1997: Gravity anomalies and spatial variations of flexural rigidity at mountain ranges. J. Geophys. Res. Solid Earth, **102**, B3, 5327–5352, doi: 10.1029/96JB03664.

Straume E. O., Gaina C., Medvedev S., Hochmuth K., Gohl K., Whittaker J. M., Abdul Fattah R., Doornenbal J. C., Hopper J. R., 2019: GlobSed: Updated Total Sediment

Thickness in the World's Oceans. Geochem. Geophys. Geosyst., **20**, 4, 1756–1772, doi: 10.1029/2018GC008115.

Subrahmanyam C., Gireesh R., Chand S., Kamesh Raju K. A., Gopala Rao D., 2008: Geophysical characteristics of the Ninetyeast Ridge–Andaman island arc/trench convergent zone. Earth Planet. Sci. Lett., **266**, 1-2, 29–45, doi: 10.1016/j.epsl.2007.10.016.

Swain C. J., Kirby J. F., 2003: The effect of 'noise' on estimates of the elastic thickness of the continental lithosphere by the coherence method. Geophys. Res. Lett., **30**, 11, 1574, doi: 10.1029/2003GL017070.

Swain C. J., Kirby J. F., 2006: An effective elastic thickness map of Australia from wavelet transforms of gravity and topography using Forsyth's method. Geophys. Res. Lett., **33**, 2, L02314, doi: 10.1029/2005GL025090.

Tassara A., 2005: Interaction between the Nazca and South American plates and formation of the Altiplano–Puna plateau: Review of a flexural analysis along the Andean margin ($15° - 34°$S). Tectonophysics, **399**, 1-4, 39–57, doi: 10.1016/j.tecto.2004.12.014.

Tassara A., Swain C., Hackney R., Kirby J., 2007: Elastic thickness structure of South America estimated using wavelets and satellite-derived gravity data. Earth Planet. Sci. Lett., **253**, 1-2, 17–36, doi: 10.1016/j.epsl.2006.10.008.

Tenzer R., Vajda P., 2009: Global atmospheric effects on the gravity field quantities. Contrib. Geophys. Geod., **39**, 3, 221–236, doi: 10.2478/v10126-009-0008-2.

Tenzer R., Hamayun K., Vajda P., 2009a: Global maps of the CRUST 2.0 crustal components stripped gravity disturbances. J. Geophys. Res. Solid Earth, **114**, B5, doi: 10.1029/2008JB006016.

Tenzer R., Hamayun K., Vajda P., 2009b: A global correlation of the step-wise consolidated crust-stripped gravity field quantities with the topography, bathymetry, and the CRUST 2.0 Moho boundary. Contrib. Geophys. Geod., **39**, 2, 133–147, doi: 10.2478/v10126-009-0006-4.

Tenzer R., Novák P., Gladkikh V., 2011: On the accuracy of the bathymetry-generated gravitational field quantities for a depth-dependent seawater density distribution. Stud. Geophys. Geod., **55**, 4, 609–626, doi: 10.1007/s11200-010-0074-y.

Tenzer R., Bagherbandi M., Gladkikh V., 2012a: Signature of the upper mantle density structure in the refined gravity data. Comput. Geosci., **16**, 4, 975–986, doi: 10.1007/s10596-012-9298-y.

Tenzer R., Novák P., Gladkikh V., 2012b: The bathymetric stripping corrections to gravity field quantities for a depth-dependent model of seawater density. Mar. Geod., **35**, 2, 198–220, doi: 10.1080/01490419.2012.670592.

Tenzer R., Gladkikh V., 2014: Assessment of density variations of marine sediments with ocean and sediment depths. Sci. World J., **2014**, doi: 10.1155/2014/823296.

Tenzer R., Chen W., Tsoulis D., Bagherbandi M., Sjöberg L. E., Novák P., Jin S., 2015: Analysis of the refined CRUST1. 0 crustal model and its gravity field. Surv. Geophys., **36**, 1, 139–165, doi: 10.1007/s10712-014-9299-6.

Tenzer R., Chen W., 2019: Mantle and sub-lithosphere mantle gravity maps from the LITHO1.0 global lithospheric model. Earth-Sci. Rev., 194, 38–56, doi: 10.1016/j.earscirev.2019.05.001.

Tesauro M., Kaban M. K., Cloetingh S. A. P. L., 2013: Global model for the lithospheric strength and effective elastic thickness. Tectonophysics, **602**, 78–86, doi: 10.1016/j.tecto.2013.01.006.

Tesauro M., Kaban M. K., Petrunin A. G., El Khrepy S., Al-Arifi N., 2018: Strength and elastic thickness variations in the Arabian Plate: A combination of temperature, composition and strain rates of the lithosphere. Tectonophysics, **746**, 398–411, doi: 10.1016/j.tecto.2017.03.004.

Tiwari V. M., Mishra D. C., 1999: Estimation of effective elastic thickness from gravity and topography data under the Deccan Volcanic Province, India. Earth Planet. Sci. Lett., **171**, 2, 289–299, doi: 10.1016/S0012-821X(99)00155-7.

Tiwari V. M., Diament M., Singh S. C., 2003: Analysis of satellite gravity and bathymetry data over Ninety-East Ridge: Variation in the compensation mechanism and implication for emplacement process. J. Geophys. Res. Solid Earth, **108**, B2, 2109, doi: 10.1029/2000JB000047.

Tiwari V. M., Grevemeyer I., Singh B., Morgan J. P., 2007: Variation of effective elastic thickness and melt production along the Deccan–Reunion hotspot track. Earth Planet. Sci. Lett., **264**, 1-2, 9–21, doi: 10.1016/j.epsl.2007.08.023.

Torsvik T. H., Amundsen H., Hartz E. H., Corfu F., Kusznir N., Gaina C., Doubrovine P. V., Steinberger B., Ashwal L. D., Jamtveit B., 2013: A Precambrian microcontinent in the Indian Ocean. Nat. Geosci., **6**, 3, 223–227, doi: 10.1038/ngeo1736.

Trivedi D., Maji T. K., Sengupta D., Nair R. R., 2012: Reappraisal of effective elastic thickness in the south-west Indian Ocean, and its possible implications. Ann. Geophys., **55**, 2, doi: 10.4401/ag-5171.

Turcotte D. L., Willemann R. J., Haxby W. F., Norberry J., 1981: Role of membrane stresses in the support of planetary topography. J. Geophys. Res. Solid Earth, **86**, B5, 3951–3959, doi: 10.1029/JB086iB05p03951.

Turcotte D., Schubert G., 2014: Geodynamics (3rd edition). Cambridge University Press, 636 p.

Vajda P., Ellmann A., Meurers B., Vaníček P., Novák P., Tenzer R., 2008: Global ellipsoid-referenced topographic, bathymetric and stripping corrections to gravity disturbance. Stud. Geophys. Geod., **52**, 1, 19–34, doi: 10.1007/s11200-008-0003-5.

Vaníček P., Tenzer R., Sjöberg L. E., Martinec Z., Featherstone W. E., 2005: New views of the spherical Bouguer gravity anomaly. Geophys. J. Int., **159**, 2, 460–472, doi: 10.1111/j.1365-246X.2004.02435.x.

Vernant P., Nilforoushan F., Hatzfeld D., Abbassi M. R., Vigny C., Masson F., Nankali H., Martinod J., Ashtiani A., Bayer R., Tavakoli F., Chéry J., 2004: Present-day crustal deformation and plate kinematics in the Middle East constrained by GPS measurements in Iran and northern Oman. Geophys. J. Int., **157**, 1, 381–398, doi: 10.1111/j.1365-246X.2004.02222.x.

Walcott R. I., 1970: Flexure of the lithosphere at Hawaii. Tectonophysics, **9**, 5, 435–446, doi: 10.1016/0040-1951(70)90056-9.

Watts A. B., Talwani M., 1974: Gravity anomalies seaward of deep-sea trenches and their tectonic implications. Geophys. J. Int., **36**, 1, 57–90, doi: 10.1111/j.1365-246X.1974.tb03626.x.

Watts A. B., 1978: An analysis of isostasy in the world's oceans, Part 1. Hawaiian–Emperor Seamount chain. J. Geophys. Res. Solid Earth, **83**, B12, 5989–6004, doi: 10.1029/JB083iB12p05989.

Watts A. B., Bodine J. H., Steckler M. S., 1980: Observations of flexure and the state of stress in the oceanic lithosphere. J. Geophys. Res. Solid Earth, **85**, B11, 6369–6376, doi: 10.1029/JB085iB11p06369.

Watts A. B., 2001: Isostasy and Flexure of the Lithosphere. Cambridge University Press, 480 p.

Wessel P., 1992: Thermal stresses and the bimodal distribution of elastic thickness estimates of the oceanic lithosphere. J. Geophys. Res. Solid Earth, **97**, B10, 14177–14193, doi: 10.1029/92JB01224.

Zingerle P., Brockmann J. M., Pail R., Gruber T., Willberg M., 2019: The polar extended gravity field model TIM_R6e. GFZ Data Services, doi: 10.5880/ICGEM.2019.005.

Zuber M. T., Bechtel T. D., Forsyth D. W., 1989: Effective elastic thickness of the lithosphere and the mechanisms of isostatic compensation in Australia. J. Geophys. Res. Solid Earth, **94**, B7, 9353–9366, doi: 10.1029/JB094iB07p09353.